

# Multi-modal matching of 2D images with 3D medical data

## Inauguraldissertation

zur

Erlangung der Würde eines Doktors der Philosophie  
vorgelegt der  
Philosophisch-Naturwissenschaftlichen Fakultät  
der Universität Basel

von

Natalia Chicherova  
aus Russland

Basel, 2018

Originaldokument gespeichert auf dem Dokumentenserver der Universität Basel  
[edoc.unibas.ch](http://edoc.unibas.ch)

Genehmigt von der Philosophisch-Naturwissenschaftlichen Fakultät auf Antrag  
von:

Prof. Dr. Bert Müller, Fakultätsverantwortlicher

Prof. Dr. Thomas Jung, Korreferent

Prof. Dr.-Ing. Andreas Maier, Korreferent

Basel, den 20. Juni 2017

Prof. Dr. Martin Spiess, Dekan

## Summary

Image registration is the process of aligning images of the same object taken at different time points or with different imaging modalities with the aim to compare them in one coordinate system. Image registration is particularly important in biomedical imaging, where a multitude of imaging modalities exist. For example, images can be obtained with X-ray computed tomography (CT) which is based on the object's X-ray beam attenuation whereas magnetic resonance imaging (MRI) underlines its local proton density. The gold standard in pathology for tissue analysis is histology. Histology, however, provides only 2D information in the selected sections of the 3D tissue. To evaluate the tissue's 3D structure, volume imaging techniques, such as CT or MRI, are preferable. The combination of functional information from histology with 3D morphological data from CT is essential for tissue analysis. Furthermore, histology can validate anatomical features identified in CT data. Therefore, the registration of these two modalities is indispensable to provide a more complete overview of the tissue. Previously proposed algorithms for the registration of histological slides into 3D volumes usually rely on manual interactions, which is time-consuming and prone to bias. The high complexity of this type of registration originates from the large number of degrees of freedom. The goal of my thesis was to develop an automatic method for histology to 3D volume registration to master these challenges.

The first stage of the developed algorithm uses a scale-invariant feature detector to find common matches between the histology slide and each tomography slice in a 3D dataset. A plane of the most likely position is then fitted into the feature point cloud using a robust model fitting algorithm.

The second stage builds upon the first one and introduces fine-tuning of the slice position using normalized Mutual Information (NMI). Additionally, using previously developed 2D-2D registration techniques we find the rotation and translation of the histological slide within the plane. Moreover, the framework takes into account any potential nonlinear deformations of the histological slides that might occur during tissue preparation.

The application of the algorithm to MRI data is investigated in our third work. The developed extension of the multi-modal feature detector showed promising results, however, the registration of a histological slide to the direct MRI volume remains a challenging task.



## Acknowledgements

During my doctoral thesis I received a lot of support from different people and I want to use the opportunity to thank them all - my colleagues, my family, my friends and everyone who helped me during this complicated period. In particular, I would like to thank both of my supervisors who directed me through my research. I am very thankful to Professor Philippe Cattin, whose brilliant scientific ideas and lively optimism helped this work to become true. I am equally thankful to Professor Bert Müller for widening my expertise and understanding of my research problem. Thanks a lot for giving me an opportunity to participate in data acquisition at Synchrotron Facilities and in histological sectioning. Also I am very grateful to my co-supervisor Dr. Simone Hieber for guidance in the project. Her attentiveness to details and deep understanding helped me a lot in my study.

I want to thank all members of the Biomaterials Science Center. Though I was only a part of my time in this group, I received full support and found good friends. Thank you very much for making me welcome in your group and for high quality data which made the project successful. I want to express my deep attachment to the Center of medical Image Analysis and Navigation. It was a great joy to be part of your team and I will miss a lot our time together.

I would like to express my gratefulness to Antal Horváth for valuable mathematical corrections, Benedikt Bitterli for the exceptional skills in speeding up a code, Adrian Schneider and Stephan Wyder for unforgettable coffee discussions as well as Simon Pezold, Simon Andermatt and Peter von Niederhäusern for patience in the office room.

Last but not least, I want to thank my parents for their unconditional love, my dear husband who supports and adores me and my son who makes me smile no matter what.



# Contents

<b>Summary</b>	<b>i</b>
<b>Acknowledgements</b>	<b>iii</b>
<b>1 Introduction</b>	<b>1</b>
1.1 Motivation . . . . .	1
1.2 Contribution . . . . .	2
1.3 Outline . . . . .	3
<b>2 Background</b>	<b>5</b>
2.1 2D-3D image registration . . . . .	5
2.2 Previous work . . . . .	8
<b>3 Publications</b>	<b>10</b>
3.1 Histology to $\mu$ CT Data Matching using Landmarks and a Density Biased RANSAC	10
3.2 Automatic Deformable Registration of Histological Slides to $\mu$ CT volume data .	19
3.3 Automatic 2D-3D Registration of Histology, MRI and CT Data . . . . .	33
<b>4 Discussion</b>	<b>47</b>





# Chapter 1

## Introduction

There is an unmet need for accurate and robust image processing methods in science and medicine. My thesis contributes to the field by developing an automatic multi-modal 2D to 3D image registration method.

### 1.1 Motivation

The motivation for my project comes from a dental study that was performed in our group. In this study by [Stalder et al. \[2014\]](#), the authors compared osteogenic potential of several bone grafting materials after a tooth extraction. In order to analyze integration of the grafting material in patients' jaws, cylindrical biopsies were extracted with a trephine bur. The entire sample volume was obtained using  $\mu$ CT which was followed by histological sectioning. To extrapolate the histological findings from 2D images to 3D volume, registration of the slide to  $\mu$ CT data was needed. The registration also enabled to determine if the histological slide was representative for the entire specimen. Moreover, based on the joint histogram of the registered images, it is possible to subdivide soft and hard tissue [[Stalder et al., 2014](#), [Schulz et al., 2010](#)]. In our group, registration of a histological slide to a 3D volume so far has been performed manually. The expert-based search of the corresponding slice in the volume is a very time-consuming task that can take up to one day per slide. Moreover, manual results may vary from

expert to expert and are hardly reproducible. Therefore, an automatic approach to register histological slides to 3D data was highly desired. The most popular methods for histology to 3D registration either rely on manual interaction, inclusion of artificial landmarks or additional modalities such as blockface images. These methods could not be applied to our problem as there were no artificial landmarks that could be easily segmented, no additional modality, and manual corrections were not appreciated either. Therefore, my thesis aimed at filling this gap and providing a versatile automated solution for registration of 2D histological slides to 3D  $\mu$ CT data.

## 1.2 Contribution

The contribution of the thesis consists of three parts. First, we developed an approach to find the best estimate of a histological slide's position and tilt in 3D space [Chicherova et al., 2014]. The most important advantages of our algorithm are that it does not require manual interaction and it can find slices under arbitrary tilt up to  $25^\circ$ . The core element of the pipeline is the feature detector. Therefore we evaluated different feature detection algorithms. The performance analysis of the three most efficient detectors is summarized in our recent work [Chicherova et al., 2016]. We found that the feature detector Speeded-up Robust Features (SURF) produces the most robust results compared to the selected detectors. Moreover, in this work we applied our pipeline to three X-ray tomography datasets of a human cerebellum biopsy. We showed that our 2D-3D localization method is robust to change of contrast and tissue type.

After analyzing the results of the first framework we noticed that a number of the estimated plane positions of histological slides could be improved. Hence, we extended the pipeline with an optimization of the slice parameters in 3D space performing a more reliable registration of the histology slide to the 3D volume. Two types of frameworks were developed – rigid and deformable. The difference between these frameworks is that in the rigid version we optimized the positioning of the plane, i.e. three degrees of freedom, and in the deformable version, we

allowed for more degrees of freedom. We complemented the three Cartesian basis vectors with Legendre polynomial basis functions. The registration of the soft tissue specimens benefits from the deformable framework, due to nonrigid deformation occurring during specimen re-embedding it could not be modeled by a plane [Khimchenko et al., 2016]. The rigid approach was evaluated on 10 jaw-bone datasets. The method localized 81 % of histological sections with a median position error of  $8.4 \mu\text{m}$ . The elastically deformable framework was evaluated on a cerebellum dataset where it improved slice localization by  $33 \mu\text{m}$  [Chicherova et al., 2017b].

Last, we automatically validated the rigid framework on 3D  $\mu\text{CT}$  and  $\mu\text{MRI}$  datasets [Chicherova et al., 2017a]. In contrast to the previous studies, here, we compared the registered parameters to automatically generated ground truth, hence, leaving out any bias from evaluation. An important contribution of this work is an extension of the feature detection strategy based on Self-similarity descriptor ( $SS$ ) [Shechtman and Irani, 2007] that we called  $SL_1$ . Our master student Khalili [2015] showed that using  $SS$  descriptor performed better in most of the jaw bone datasets. More importantly, the  $SS$  descriptor is built on local correlation in an image, hence, more suitable for multi-modal matching. Based on these ideas we combined the rotation invariant self-similarity descriptor and  $L_2$  and  $L_1$ -norm outlier rejection. The densely extracted  $SL_1$  descriptor made it possible to take into account homogeneous areas of the tissue where SURF was not able to detect features. Additionally, we registered one histological slide to the two datasets. We found that histology to the  $\mu\text{CT}$  registration is more reliable than histology to the  $\mu\text{MRI}$  where the gray value gradient is very different from the histological one. Reasonable registration of the slide could be achieved through the 3D-3D registration of the  $\mu\text{CT}$  and  $\mu\text{MRI}$ .

## 1.3 Outline

In Chapter 2, we outline the most important studies in the field of 2D-2D and 2D-3D registration. The variety of rigid and nonrigid techniques in combination with dense and sparse similarity measures were previously applied to the problem. In Section 2.2, we introduce a

multi-modal 2D histology to 3D data registration and describe the main challenges that need to be faced.

Chapter 3 combines the main paper contributions. In Section 3.1, the first pipeline for localizing a histological slide in a 3D volume is presented. The automatization of an initial slide position is achieved using a combination of fast feature detection and a robust plane fitting. Further improvement of the algorithm is described in Section 3.2 where we show that coarse to fine registration strategy can achieve better results. Moreover, we propose a solution for nonlinear deformations of the histological slide using polynomials. Lastly, in Section 3.3, we present an attempt to extend an application of the algorithm to histology and MRI data registration and propose a potential feature detection approach, namely  $SL_1$ , to solve it.

Chapter 4 discusses the limitations of the algorithm and outlines future work to overcome them.

# Chapter 2

## Background

### 2.1 2D-3D image registration

Matching images acquired with different modalities (multi-modal images) plays an important role in biomedical research. Alignment of the images or registration is a process of bringing images to a consistent coordinate system. In other words, registration can be defined as finding a geometric transformation that maps points from one image to points in another image. The variety of image transformation techniques include basic linear transformation (translation, rotation, affine) as well as more sophisticated nonlinear ones such as thin-plate splines, polynomials, a B-splines [Pluim et al., 2003].

Registration methods can be classified with respect to the chosen similarity measure into intensity based and landmark based. In intensity based approaches the similarity metric is calculated by taking every pixel value of an image into account. Most commonly used metrics are Mean Squared Distance, Normalized Cross-correlation or Mutual Information (MI) [Viola and Wells III, 1997]. These metrics are able to align images with very high accuracy, however, due to dense sampling are time consuming for large scale data. In contrast, landmark based approaches find distinctive features which represent the entire image with a sparse set of points. The matching of the images is then reduced to calculating distances between the descriptor vectors of these features.

Another way to classify the registration methods is based on data dimensionality, i.e. 2D-2D, 3D-3D and 2D-3D methods. A large variety of techniques to register data of consistent dimensionality (2D-2D and 3D-3D) has been published [Pluim et al., 2003]. For example, various techniques for 3D-3D registration are based on MI as a measure of similarity between images, e.g. registration of MRI and CT volumes [Andronache et al., 2008], PET and MRI [Maes et al., 1997]. The 2D-2D rigid approaches are often based on feature point correspondence (landmark based). A mapping function for every pixel from one image to another is then found using a set of correspondences.

One of the most common approaches to estimate the mapping function is called RANSAC Homography [Fischler and Bolles, 1981]. This algorithm finds a transformation matrix by randomly selecting four point pairs among the found correspondences. The coordinates of the points are then used to solve a linear system of equations and to calculate the values of the transformation matrix  $H$  (Eq. 2.1). Hence, every point of one image  $P_I = (x_i, y_i)$  is transformed to a point in the other image  $P_J = (x_i, y_i)$  by multiplying with the matrix  $H$  (Eq. 2.1), where  $i$  goes through all the corresponding points in the image  $I$  or  $J$ .

$$\begin{pmatrix} x_i^J \\ y_i^J \\ 1 \end{pmatrix} = \underbrace{\begin{pmatrix} h_{1,1} & h_{1,2} & h_{1,3} \\ h_{2,1} & h_{2,2} & h_{2,3} \\ h_{3,1} & h_{3,2} & h_{3,3} \end{pmatrix}}_{:=H} \begin{pmatrix} x_i^I \\ y_i^I \\ 1 \end{pmatrix}. \quad (2.1)$$

Due to its robustness, the RANSAC Homography algorithm became the state of the art technique in many image analysis fields. The key to the robust performance lies in iterative thresholding of false feature correspondences (outliers). The final transformation matrix  $H$  is then calculated based on correctly matched features (inliers). Another robust approach for 2D-2D rigid registration was recently proposed by Ask et al. [2014]. It determines rotation and translation between the matching points using their absolute distance or  $L_1$ -norm. There also exist numerous non-rigid methods for 2D-2D registration [Kybic and Unser, 2003, Andronache et al., 2008, Heinrich et al., 2012].

Although a wide variety of these techniques have been proposed in the literature, the multi-modal 2D-3D registration remains a challenging problem. A recent review by [Markelj et al., 2012] outlines main 2D-3D registration approaches used for image-guided surgeries. The suggested approaches mainly address registration of 2D fluoroscopy projections with 3D computed tomography volumes. This, however, makes these approaches not entirely multi-modal because both of the modalities utilize an X-ray source for image acquisition. Several reviewed methods investigate 2D fluoroscopy to MRI volume registration [Fei et al., 2003, Bullitt et al., 1999]. Most of the proposed 2D-3D registration techniques are based on contour or surface alignment and consequently require segmentation. The segmentation, in turn, is often data specific or utilizes manual correction, hence, not desired in the framework.

Another type of 2D-3D multi-modal registration is concerned with aligning optical microscopy images with 3D data such as CT or MRI. The need for 2D microscopy to 3D volume registration is growing fast with the arrival of novel image acquisition techniques and increase of application in biomedicine. Indeed, microscopy imaging is a gold standard technique in such fields as cancer research, dentistry or bacteriology. For example, histological sectioning is a usual procedure to analyze jaw bone biopsies.

Histological sectioning can be reduced to three main steps. First, a slide is cut through the specimen volume. Then, the slide is stained with chemicals to highlight the tissue components of interest. And last, an optical microscopy image of this slide is taken. Histology is an essential tool to obtain functional information about the tissue which allows to differentiate between the tissue types. It also serves as a validation technique that complements other imaging modalities. However, arbitrarily selected histological cuts provide information only about a small part of the volume. To visualize the entire tissue distribution in the specimen the 3D acquisition techniques such as micro CT ( $\mu$ CT) or MRI are needed. Combining the 2D histological slides with 3D imaging modalities provides a more complete overview of functional and morphological structure of the sample. This challenging problem of 2D-3D multi-modal registration was the main focus of my research.

## 2.2 Previous work

The available works on histology slide to 3D data registration can be classified into two classes. The first class reconstructs prior to registration the 3D volume out of the histological sections and then performs 3D-3D registration [Alic et al., 2011, Nir et al., 2014, Ourselin et al., 2001]. The second class registers a single histological 2D slide to the 3D volume [Sarve et al., 2008, Hoerth et al., 2015, Wachowiak et al., 2004]. The first type is built upon the position information about the histological cut which allows reconstructing a volume from the slides. To determine this information one can use a complementary modality such as blockface photographs [Dauguet et al., 2007, Goubran et al., 2013, Kim et al., 1997, Meyer et al., 2006, Park et al., 2008, Schormann and Zilles, 1998, Uberti et al., 2009] or photographs of an unstained sample [Yelnik et al., 2007]. Other studies rely on implanted artificial markers [Breen et al., 2005, Humm et al., 2003, Lazebnik et al., 2003] or colour-coding [Alic et al., 2011]. However, all these techniques make the histological sectioning procedure more labor intensive, and the additional facilities are not always available in the laboratory. Other algorithms reconstruct the volume using segmentation, which is then used for distance minimization between contours [Ou et al., 2009, Taylor et al., 2004, Zhan et al., 2007] or for more robust similarity measure calculation [Mosalganti et al., 2008, Nir et al., 2014, Ourselin et al., 2001, Seise et al., 2011]. To summarize, the 3D histology volume to 3D CT or MRI data registration approaches are a reasonable choice in case of serial histological sectioning and availability of additional imaging modalities. They are also very useful when the data are easily segmented.

Limited amount of research has also been done on 2D-2D registration of histology to CT, MRI or US slices [Andronache et al., 2008, Arganda-Carreras et al., 2010, du Bois d'Aische et al., 2005, Li et al., 2006, Pitiot et al., 2003]. Li et al. [2006] performed coarse-to-fine registration of histology and 2D MRI slices. Starting with affine transformation non-rigid thin plate spline registration was applied based on manual corresponding landmarks.

In this thesis we concentrate on a more challenging type of histology registration that is a single slice-to-volume registration. In contrast to the methods described above, here, there is only one slide available. Hence there is no information to compensate for rotation and translation as



in serial sectioning. Second, the position of the slice in 3D space is not known. The aforesaid reason is in fact the main challenge of the field and according to our knowledge so far no automatic solution existed. For example, a recently proposed algorithm based on generalized Hough transform provides a semi-automatic solution to the slice-to-volume registration [Hoerth et al., 2015]. In another study by Sarve et al. [2008], the authors first minimized edge distances between a segmented implant to find a position of histology in 3D  $\mu$ CT. Then, registration was achieved by rotating the histological slide around the main axis of the implant. The best slice was selected in the interval  $\pm 20^\circ$  by choosing the one with the highest normalized MI (NMI). In Wachowiak et al. [2004] the authors investigated a global optimization algorithm for rigid registration of a 3D histology stack to 2D tomograms and ultrasound images. The paper gave an extensive assessment of the performance for different global optimization algorithms and presented an adapted evolutionary approach called particle swarm optimization. Nonlinear deformations perpendicular to the slicing plane are also explored in the literature [Dauguet et al., 2007, du Bois d’Aische et al., 2005, Goubran et al., 2015, Kim et al., 2000, Schormann et al., 1995]. However, only some of them investigated nonrigid registration techniques in application to histology [Dauguet et al., 2007, Goubran et al., 2015, Osechinskiy and Kruggel, 2010, Schormann and Zilles, 1998]. A general framework for slice deformation in 3D space was evaluated by Osechinskiy and Kruggel [2010] for different registration techniques and an optimal set of parameters was identified. Non-rigid 2D-3D registration was also investigated by Kim et al. [2000]. They used non-linear polynomial functions to relate the coordinates of 2D histology to 3D MRI. By calculating the intensity difference between voxels, coefficients of polynomials were optimized. The initialization for the optimization was calculated based on the minimal value of the similarity measure along the MRI volume, which is sub-optimal in case of high similarity within the volume. The described methods for the slice-to-volume registration achieve reasonable results and require minimal manual intervention either at the stage of segmentation or registration initialization.

# Chapter 3

## Publications

### 3.1 Histology to $\mu$ CT Data Matching using Landmarks and a Density Biased RANSAC

Natalia Chicherova, Ketut Fundana, Bert Müller, Philippe Cattin

In the following paper we introduced an automatic algorithm that finds a position of a 2D histological slide in a 3D  $\mu$ CT data.

**Authors contribution.** Natalia Chicherova and Prof. Philippe Cattin equally contributed to the algorithm development, figure design, data analysis and wrote the main parts of the manuscript. The implementation of the pipeline was performed by Natalia Chicherova. Dr. Ketut Fundana contributed to the algorithm development and manuscript writing. Prof. Bert Müller provided the data. Prof. Philippe Cattin and Prof. Bert Müller designed the study.

# Histology to $\mu$ CT Data Matching Using Landmarks and a Density Biased RANSAC

Natalia Chicherova<sup>1,2</sup>, Ketut Fundana<sup>1</sup>, Bert Müller<sup>2</sup>, and Philippe C. Cattin<sup>1</sup>

<sup>1</sup> Medical Image Analysis Center, University of Basel, Basel, Switzerland

<sup>2</sup> Biomaterials Science Center, University of Basel, Basel, Switzerland

natalia.chicherova@unibas.ch

**Abstract.** The fusion of information from different medical imaging techniques plays an important role in data analysis. Despite the many proposed registration algorithms the problem of registering 2D histological images to 3D CT or MR imaging data is still largely unsolved.

In this paper we propose a computationally efficient automatic approach to match 2D histological images to 3D micro Computed Tomography data. The landmark-based approach in combination with a density-driven RANSAC plane-fitting allows efficient localization of the histology images in the 3D data within less than four minutes (single-threaded MATLAB code) with an average accuracy of 0.25 mm for correct and 2.21 mm for mismatched slices. The approach managed to successfully localize 75% of the histology images in our database. The proposed algorithm is an important step towards solving the problem of registering 2D histology sections to 3D data fully automatically.

## 1 Introduction

Image registration is the art of automatically aligning or warping medical imaging data. Registered data allows a more in depth analysis of the probed tissues as different modalities often represent different physical properties important to better understand and interpret the data at hand. Many approaches have been proposed in the last decades for 2D-to-2D and 3D-to-3D registration of the same or even different modalities [11]. However, registering 2D histological images to 3D data is a largely unexplored problem.

The need for reasonable 2D histology to 3D data registration becomes more and more important with the availability of affordable micro Computed Tomography ( $\mu$ CT) devices with high spatial resolution and tissue contrast. Combining the functional information from histology with the structural imaging data of the  $\mu$ CT provides better insights in identifying anatomical features of hard and soft tissues.

Only few papers are insofar directly related to the research at hand as they describe the registration of histological sections to CT and MR data. Seise *et al.* [9] proposed an interactive registration of histological sections to CT in the context of radiofrequency ablation. However, this approach highly relied on manual intervention in the registration step as well as in segmentation. Sarve *et al.* [8]

registered histological images of bone implants with synchrotron radiation-based  $\mu$ CT data. Their algorithm was based on segmentation of the implant by thresholding, which is not possible in our datasets, as the implant material is hardly visible and highly assimilated in the jaw bone. Other approaches deal with the registration of histological sections with soft tissue such as in the prostate [7] or the human brain [6] where MRI is more useful than CT. An additional factor is that the acquired  $\mu$ CT or  $\mu$ MR imaging data is generally of large size, amounting up to several hundred megabytes of data. However, only very little research has been devoted to efficiently register these type of datasets [5].

Using images of histological cross sections poses additional challenges to the already ill-posed problem of image registration. First, the histology images are susceptible to uneven lighting (vignetting artifact) and different contrasts from staining. Second, the histological sections may suffer from severe non-rigid deformations originating from the cutting process. Moreover, the histological images generally show different contrasts as compared to the  $\mu$ CT or  $\mu$ MR data that must be handled appropriately. Lastly, the potentially non-uniform background of the histological cuts may lead to erroneous results in the registration process.

In this paper we propose a novel approach for automatic registration of 2D histological cross sections to 3D  $\mu$ CT scans. This fully automatic feature-based registration approach makes use of the scale- and rotation-invariant feature detector SURF[2] and a modified density-driven RANSAC[3] plane-fitting. The main advantage of our method is that it can detect corresponding slices under different angulation that often appears in histological sectioning experiments. Furthermore, the computation time of our algorithm is notably shorter than of manual registration. The latter is estimated at 8 hours per slice. Finally, it does not require insertion of any additional landmarks hence can be readily applied to numerous biological data, where auxiliary inclusions are impossible.

## 2 Method

An illustration of the algorithmic pipeline is depicted in the Fig. 1. First, we determine corresponding feature points between the histological image and each image in the  $\mu$ CT volumetric data and extract their associated coordinates. Then, based on these coordinates, we build a 3D point cloud, where the third dimension corresponds to the slice number in the  $\mu$ CT data. As the distribution of the matched points is higher in the plane that corresponds best to a given histological slice (see Fig. 1(middle)) the remaining step reduces to a robust plane fitting in a noisy point cloud.

### 2.1 Data Acquisition

The sample data used for this work [10] originates from a jaw bone volume augmentation after tooth extraction study. In total ten clinical patients were included in this study. Biopsies of the jaw bones were taken from 4 to 11 months after implantation. The inner diameter of the specimen tubes was around 3 mm

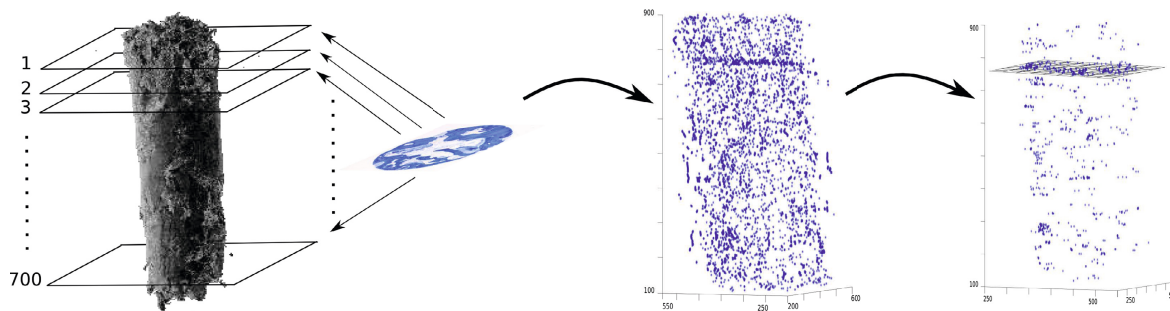


**Fig. 1.** Pipeline of the algorithm: (left) Feature matching of  $\mu$ CT data and histological image, (middle) 3D point cloud of matched points, (right) optimized RANSAC plane fitting

and the length was around 12 mm. The  $\mu$ CT of the whole specimen was acquired. Then five to nine histological cross-sections through the horizontal plane of the specimen were taken. Each histological slice (thickness  $300\ \mu\text{m}$ ) resulted in an RGB image of size  $2592 \times 1944$  pixels. The  $\mu$ CT data were 8 bit gray-scale 3D matrices with a range of data size  $764 \times 764 \times (416 \div 1939)$  pixels, where the vertical axis corresponds to the third dimension. The corresponding resolution along vertical axis differed from 0.03 mm to 0.006 mm per slice.

## 2.2 Feature Detection and Matching

Let  $I(x, y)$  and  $V(x, y, z)$  denote the histological image and the  $\mu$ CT data volume accordingly, where  $z$  is associated with a slice number in the  $\mu$ CT dataset. Hence,  $I : \Omega_I \subset R^2 \rightarrow R$  and  $V : \Omega_V \subset R^3 \rightarrow R$ . The rigid registration problem between these two modalities can be formulated as finding coefficients of the plane section in the  $\mu$ CT space that corresponds best to the histological image. In a first step we match each of the histological images to all axial  $\mu$ CT slices using a landmark-based approach. As a feature detection algorithm we rely on the scale- and rotation-invariant feature detector and descriptor SURF [2]. The choice of this detector is based on performed comparative analysis with SIFT[4]. We have found that SURF was more accurate and computationally efficient for our application. For a Matlab implementation of the SURF algorithm we used the opensource code by D. Kroon of Sep 2010<sup>1</sup>, saving the default parameters. The number of octaves was set to 5, threshold to 0.0002. The main principal of this detector is based on scale-space extrema detection and stable feature localization. Applying the feature detector to an image, *e.g.* histological image  $I$ , we obtain a small subset of distinctive feature points  $P(x, y) \subset I$ . The descriptor vectors are then used for matching the feature points between the  $\mu$ CT and histological images. As the matching algorithm, we use the second-nearest-neighbor-criteria [4,1] that calculates the Euclidean distance between the descriptor vectors. A match is only accepted when the smallest Euclidean distance is less than 0.8

<sup>1</sup> <http://www.mathworks.ch/matlabcentral/fileexchange/28300-opensurf--including-image-warp->

times the second smallest Euclidean distance. This process is then repeated for all the axial slices in the  $\mu$ CT dataset.

### 2.3 The 3D Feature Point Cloud

Suppose that the result of the above matching step is a set of feature points  $P_z \subset V_z$  with coordinates  $(x_i, y_i)$ , where  $i = 1 \dots \kappa_j$  and  $\kappa_j$  is the number of found matching feature points in a slice  $z$ . Having matched features for each of the  $N$  slices in the  $\mu$ CT volume will subsequently allow us to plot them as a point cloud, *i.e.* the 3D set of the keypoints  $C = \{(x_{ij}, y_{ij}, z_j)\}$  ( $j = 1 \dots N$ ) with the third dimension  $z$  representing the slice number in the  $\mu$ CT data, see Fig. 1(middle). Here, the total number of feature points for the whole  $\mu$ CT data is determined as  $M = \sum_{j=1}^N \kappa_j$ .

As one would expect, the resulting point cloud shows an increased density of found matches at the correct location of the histology section. This holds true even for histological images that are tilted with respect to the  $z$ -axis of the  $\mu$ CT dataset. This plane - well visible in the point cloud of Fig. 1(middle) - corresponds to the best position for the histological slice. In order to efficiently extract the plane parameters, we define a binary matrix  $B(x, y, z) : \Omega_V \subset R^3 \rightarrow R$  as

$$B(x, y, z) = \begin{cases} 1 & \text{if } (x, y, z) \in C \\ 0 & \text{otherwise,} \end{cases}$$

which is then convolved with a 3D Gaussian as  $B_\sigma = G_\sigma * B$ . Thus, in each point we obtain a new intensity value that is influenced by the neighboring keypoint distribution across the  $\mu$ CT space and thus reflects the local density of matched points.

### 2.4 Density-Driven RANSAC for Robust Plane Fitting

One of the most widely used robust algorithms for extracting shapes from a data set with outliers is RANSAC [3]. The algorithm randomly selects a minimum number of points that uniquely defines a fitting shape. Then the corresponding primitive is constructed. In our problem, the model of interest is a plane  $Ax + By + Cz + D = 0$  and the minimum number of points is 3. Therefore, the output parameter of the algorithm is a four dimensional normal vector  $\mathbf{n} = [A \ B \ C \ D]^T$ . RANSAC then counts the number of points within the distance threshold  $t$  to the obtained candidate model (inliers). If the number of inliers for one model is larger than in the previous iteration, the new model parameters are retained. Otherwise, another subset is randomly selected. Depending on the ratio of inliers over outliers, this process has to be repeated multiple times to assure with a high probability that a solution is found when present. The large amount of outliers in our data would result in a large number of iterations.

In this work we thus propose to bias the random sampling of the RANSAC plane fitting process towards points with high density *i.e.* points that are close to the plane of interest. To optimize the plane detection algorithm, the dataset

$B_\sigma$  is further reduced to  $\rho < M$  points by retaining features with the largest density values. However, the new dataset  $B_\rho \subset B_\sigma$  still contains some outliers due to high similarities within a specimen along the vertical axis.

To further reduce the number of required sampling iterations, we bias the random sampling code towards preferring points with a higher local density. Thus points with a high local density have a higher probability of being selected. Suppose that each density value of the dataset  $B_\rho$  is assigned to the weighting vector  $\mathbf{w} = \{w_l\}$ , where  $l = 1 \dots \rho$ . Therefore, instead of using the unbiased classical sampling of the original RANSAC, the probability of picking an element  $b_m \in B_\rho$  is then defined as  $p_m = w_m / \sum_{l=1}^{\rho} w_l$ .

A further optimization is associated with the angle  $\alpha$  between the  $z$ -axis and the plane formed by the currently randomly sampled points from the dataset. Based on our observations we restrict this angle to lie between  $-\alpha_{hist} < \alpha < \alpha_{hist}$ . In other words, for every iteration, the 3D coordinates of the sampled points  $\{b_1, b_2, b_3\} \in B_\rho$  are used to calculate the normal of the plane that goes through these points  $\mathbf{n} = (b_2 - b_1) \times (b_3 - b_1)$ . We then find the angle  $\alpha = \arccos(n_z / \|\mathbf{n}\|)$ , subject to  $-\alpha_{hist} < \alpha < \alpha_{hist}$ . Therefore, only planes that satisfy this constraint are considered for further procession in RANSAC. These two modifications allow to robustly fit a plane to the selected points and to obtain its parameters. An example of the point cloud with corresponding plane fit is shown in the Fig. 1.

Finally, we make a cut through the  $\mu$ CT data matrix along the fitted plane. The image in this cut is the result of our algorithm and should be maximally similar to the histological image.

---

### Algorithm 1. 2D-3D matching

---

**Input:** Histological image  $I$  and  $\mu$ CT 3D dataset  $V$ , RANSAC threshold  $t=10$ ,  $\rho=1000$ ,  $\alpha_{hist} = \frac{\pi}{8}$

**Output:** Plane parameters  $\mathbf{n}$

Convert  $I$  to gray scale

**for all**  $V_j$ , ( $j = 1 \dots N$ ) **do** ▷ Detect coordinates of matching points

$(x_i, y_i) = SURF(I, V_j)$

Build 3D set of coordinates  $C = \{(x_{ij}, y_{ij}, z_j)\}$

**end for**

Create a binary 3D matrix  $B(x, y, z)$

**for**  $(x, y, z) \in B$  **do**

**if**  $(x, y, z) \in C$  **then**

set  $B(x, y, z)$  to 1

**end if**

**end for**

Convolve with Gaussian:  $B_\sigma = G_\sigma * B$

Find  $\rho$  highest values in  $B_\sigma$

Define  $B_\rho \subset B_\sigma$ , *i.e.* keep  $\rho$  points with the highest values

$\mathbf{n} = \text{RANSAC}(B_\rho, t, \alpha_{hist}, \mathbf{w})$  ▷ Fit a plane into  $B_\rho$  using its values as weights  $\mathbf{w}$

**return**  $\mathbf{n}$

---

### 3 Results

Our framework was validated on ten  $\mu$ CT datasets with overall 60 histological cross section images. For each histological slice we obtained a four dimensional vector which uniquely describes a plane in a 3D space. To compare the automatically found results with manually found locations we estimated the  $z$ -coordinate along the  $\mu$ CT volume and the angle between  $z$ -axis and the normal to the plane which represents a cut of the specimen. The  $z$ -coordinate was calculated as a center point of the obtained plane. All manually found matching parameters were obtained from VG studio which provides a four-dimensional vector of the searching plane and automatically computes the center point of the plane, *i.e.*,  $z$ -coordinate. We also performed a visual assessment of the automatically found images. In Fig. 2, we showed two examples of a matched slice found automatically ((a) and (d)) in comparison with manually found ((b) and (e)) and histological image ((c) and (f)). The complete result of the visual estimation with corresponding comparison with the ground truth values is summarized in Table 1. In nine out of ten datasets our approach has allocated at least half of the histological slices with an average difference of 0.25 mm. For the datasets 4, 5 and 10 the algorithm showed poor performance. The average distance for mismatched slices averaged around 286 slices and an overall accuracy for mismatched slices reached 2.21 mm. This might be due to high intensity variations within the  $\mu$ CT dataset and the inhomogeneous dying of the histological slices (see Fig. 3(a)). The extrema detector was very sensitive to intensity changes and dirt spots on the histological slices. This caused wrong feature responses and consequently incorrectly matched images.

The comparison of the angles with the ground truth is shown in Table 2. For intuitive reasons, we provided negative angles instead of angles around  $360^\circ$  to stress small alternation of the cutting section slopes. For small angles (around  $5^\circ$ ) our approach showed high efficiency, whereas, for the angles of more than  $10^\circ$ , which corresponded to 0.53 mm of the specimen, it often found only a close approximation to the desired section of the  $\mu$ CT volume. For example, for the dataset 10, it has found a very close slice number, but determined a wrong angulation.

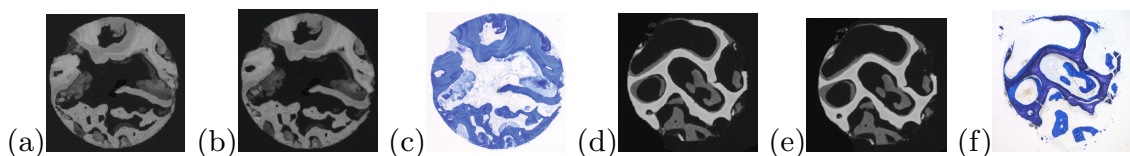


**Fig. 2.** (a),(d) Automatically found image. (b),(e) Manually found image. (c),(f) Histological image.



**Table 1.** Number of matched and mismatched images with corresponding average differences between automatically and manually found slices

Data set	1	2	3	4	5	6	7	8	9	10
Number of Matched slices	6	9	6	1	3	5	5	3	3	3
Average distance [mm]	0.06	0.04	0.9	0.17	0.05	0.59	0.24	0.07	0.16	0.13
Average difference [slices]	10	3	8	6	3	63	10	4	10	9
Number of Mismatched slices	0	0	1	4	3	1	1	1	2	3
Average distance [mm]	-	-	0.17	2.71	4.56	2.96	1.07	0.67	0.76	1.37
Average distance [slices]	-	-	15	94	286	314	45	40	47	91

\*Note that number of slices per 1 mm is different for different samples.

**Table 2.** Comparison of average automatically found angles for matched slices with manually found angles

Data set	1	2	3	4	5	6	7	8	9	10
Average automatic angle [°]	1	1	1	-23	4	-1	-4	5	5	19
Manual angles [°]	-2	-5	5	-22	4	-19	-7	19	-8	-13

## 4 Discussion

Our novel algorithm for automatic 2D-3D registration showed a very high efficiency and small computational complexity and can be readily applied to the matching problem.

However, it has certain limitations regarding the feature detection step. Despite the good feature matching performance of SURF for most images it can not be considered a multi-modal approach but rather one that is robust against lightning changes. This also explains its poor performance when matching histological sections with non-uniform intensity variations. Moreover, additional complication arose from the histological slices that were compiled from disintegrated pieces (see Fig. 3(b)) and could not be readily matched with the same specimen. To overcome these limitations we want, firstly, to focus on developing a feature detector and descriptor that better will account for these specific characteristics and will efficiently work for multi-modal 2D-3D registration. Secondly, we want to include a non-rigid deformation estimation once the initial plane has been found. Lastly, we plan on further speeding up the calculation time by parallelization and GPU implementations. With a computation time of less than four minutes on a single-threaded MATLAB implementation, the algorithm still leaves room for further optimization and parallelization. This is irrespective of any angulation between the histology sections with respect to the  $\mu$ CT data.

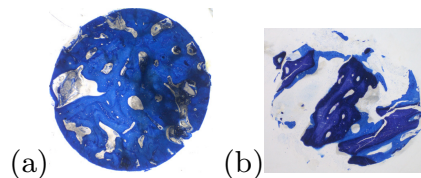


**Fig. 3.** (a) Inhomogeneous dyeing of the histological slice from the 5th dataset. (b) Compiled from pieces histological slice from the 8th dataset.

**Acknowledgements.** We would like to thank members of Biomaterials Science Center (University of Basel): Anja Stalder for the manually found slices and Simone Hieber for the help with the project. The work is funded by SNSF (project 150164).

## References

1. Baumberg, A.: Reliable feature matching across widely separated views. In: IEEE Conference on Computer Vision and Pattern Recognition, vol. 1, pp. 774–781 (2000)
2. Bay, H., Ess, A., Tuytelaars, T., Van Gool, L.: Speeded-up robust features (SURF). *Computer Vision and Image Understanding* 110, 346–359 (2008)
3. Fischler, M.A., Bolles, R.C.: Random sample consensus: a paradigm for model fitting with applications to image analysis and automated cartography. *Communications of the ACM* 24, 381–395 (1981)
4. Lowe, D.G.: Distinctive image features from scale-invariant keypoints. *International Journal of Computer Vision* 60, 91–110 (2004)
5. Mosaliganti, K., Pan, T., Sharp, R., Ridgway, R., Iyengar, S., Gulacy, A., Wenzel, P., de Bruin, A., Machiraju, R., Huang, K., et al.: Registration and 3D visualization of large microscopy images. In: *SPIE Medical Imaging*, vol. 6144 (2006)
6. Osechinskiy, S., Kruggel, F.: Slice-to-volume nonrigid registration of histological sections to MR images of the human brain. *Anatomy Research International* (2010)
7. Ou, Y., Shen, D., Feldman, M., Tomaszewski, J., Davatzikos, C.: Non-rigid registration between histological and MR images of the prostate: A joint segmentation and registration framework. In: *IEEE Computer Vision and Pattern Recognition Workshops*, pp. 125–132 (2009)
8. Sarve, H., Lindblad, J., Johansson, C.B.: Registration of 2D histological images of bone implants with 3D SR $\mu$ CT volumes. In: *Advances in Visual Computing*, pp. 1071–1080 (2008)
9. Seise, M., Alhonnoro, T., Kolesnik, M.: Interactive registration of 2D histology and 3D CT data for assessment of radiofrequency ablation treatment. *Journal of Pathology Informatics* 2, 72 (2011)
10. Stalder, A.K., Ilgenstein, B., Chicherova, N., Deyhle, H., Beckmann, F., Müller, B., Hieber, S.E.: Combined use of micro computed tomography and histology to evaluate the regenerative capacity of bone grafting materials. *International Journal of Materials Research* (2014)
11. Zitova, B., Flusser, J.: Image registration methods: a survey. *Image and Vision Computing* 21, 977–1000 (2003)


## 3.2 Automatic Deformable Registration of Histological Slides to $\mu$ CT volume data

Natalia Chicherova, Simone E. Hieber, Anna Khimchenko, Christos Bikis, Bert Müller,  
Philippe Cattin

This manuscript is an extension of the previous study. Here, we introduced a pipeline for localization improvement and complete registration of the 2D histology slide to the 3D  $\mu$ CT data.

**Authors contribution.** Natalia Chicherova contributed to the algorithm development, its implementation, data analysis, figures design and wrote the main parts of the manuscript. Dr. Simone E. Hieber contributed to the data analysis and figures drawing. The data were acquired by Anna Khimchenko (3D cerebellum volume) and Christos Bikis (histology slides) of Prof. Bert Müller group. Manual results were obtained by Anna Khimchenko, Christos Bikis, Dr. Simone E. Hieber and Natalia Chicherova. Prof. Philippe Cattin contributed to the algorithm development and figures design. Prof. Philippe Cattin and Prof. Bert Müller designed the study. All authors discussed the results, contributed to the final manuscript and reviewed it.

# Automatic deformable registration of histological slides to $\mu$ CT volume data

N. Chicherova<sup>\*,†</sup>, S.E. Hieber<sup>†</sup> , A. Khimchenko<sup>†</sup>, C. Bikis<sup>†</sup>, B. Müller<sup>†</sup> & P. Cattin<sup>\*</sup>

<sup>\*</sup>Center for medical Image Analysis & Navigation, Department of Biomedical Engineering, University of Basel, Allschwil, Switzerland

<sup>†</sup>Biomaterials Science Center, Department of Biomedical Engineering, University of Basel, Allschwil, Switzerland

**Key words.** 2D-3D registration, histology, micro computed tomography, multimodal, slice-to-volume registration.

## Summary

Localizing a histological section in the three-dimensional dataset of a different imaging modality is a challenging 2D-3D registration problem. In the literature, several approaches have been proposed to solve this problem; however, they cannot be considered as fully automatic. Recently, we developed an automatic algorithm that could successfully find the position of a histological section in a micro computed tomography ( $\mu$ CT) volume. For the majority of the datasets, the result of localization corresponded to the manual results. However, for some datasets, the matching  $\mu$ CT slice was off the ground-truth position. Furthermore, elastic distortions, due to histological preparation, could not be accounted for in this framework.

In the current study, we introduce two optimization frameworks based on normalized mutual information, which enabled us to accurately register histology slides to volume data. The rigid approach allocated 81 % of histological sections with a median position error of 8.4  $\mu$ m in jaw bone datasets, and the deformable approach improved registration by 33  $\mu$ m with respect to the median distance error for four histological slides in the cerebellum dataset.

## Introduction

Histology slides generally form the basis of a quantitative analysis of tissue morphology. Because the two-dimensional slide represents only a part of the three-dimensional object, the conclusions may depend on the slide selection, see, e.g. (Bernhardt *et al.*, 2004). Micro computed tomography ( $\mu$ CT) yields the full three-dimensional information in a nondestructive fashion and is, therefore, complementary to the histological analysis. If the morphological information is at least partially available in both data, one can extrapolate the information

from histology to the third dimension (Hieber *et al.*, 2016; Khimchenko *et al.*, 2016). Furthermore, it is well known that the preparation of histology slides gives rise to artefacts, including cracks and location-dependent shrinkage (Germann *et al.*, 2008; Schulz *et al.*, 2011). Using even less detailed CT data, one can correct the slides to obtain more reliable results. For the artefact correction, the selection of an optimized cutting direction and the extrapolation into the third dimension, a sound identification of the two-dimensional counterpart of the histological slide in the three-dimensional tomography dataset is necessary. Image registration is the basis for numerous image analysis techniques. In particular, the registration of images from different modalities enables practitioners to obtain a large amount of complementary information for accurate diagnosis (Zhan *et al.*, 2007; Alic *et al.*, 2011; Seise *et al.*, 2011; Goubran *et al.*, 2015), the combination of functional and morphological data (Schormann & Zilles, 1998; Müller *et al.*, 2012; Particelli *et al.*, 2012; Schulz *et al.*, 2012; Stalder *et al.*, 2014) or atlas construction (Ourselin *et al.*, 2001; Tsai *et al.*, 2008; Krauth *et al.*, 2010; Tsai *et al.*, 2011), to name but a few. The task is particularly challenging when aligning multimodal data of different dimensions, such as 2D to 3D. There exist many techniques for 2D projections to 3D volume registration (Markelj *et al.*, 2012). None of them can be applied to our problem, i.e. matching a histological slide to a tomographic volume dataset acquired from the same specimen, because of two main reasons. First, the basic goal of these algorithms is to find a mapping between the projections and the 3D volume. Second, the methods often require manual feature identification. In contrast, our 2D-3D registration problem is concerned with registering a 2D slide such as histological section to a 3D dataset, i.e. slide-to-volume registration. In the literature, it is commonly referred to as slice-to-volume registration (Ferrante & Paragios, 2017) and only a few approaches investigate the problem of registering 2D histology images to 3D datasets as well as 2D-2D multimodal registration of histological images (Jacobs *et al.*, 1999; du Bois d'Aische *et al.*, 2005; Li *et al.*, 2006; Pitiot *et al.*, 2006).

Correspondence to: Simone E. Hieber, Biomaterials Science Center, Department of Biomedical Engineering, University of Basel, Allschwil 4123, Switzerland. Tel: +41 61 207 54 33; fax: +41 61 207 54 99; e-mail: simone.hieber@unibas.ch

The most common approaches for registering histological sections to the 3D space initially reconstruct a 3D volume from histology serial sections and then apply 3D-3D registration (Ourselin *et al.*, 2001; Ceritoglu *et al.*, 2010; Alic *et al.*, 2011; Nir & Salcudean, 2013). Reconstructing a 3D volume from 2D histological sections, however, requires information about the sectioning location in 3D space, which is not always available. One way of determining this information is to use a complementary modality such as blockface photographs (Kim *et al.*, 1997; Schormann & Zilles, 1998; Meyer *et al.*, 2006; Dauguet *et al.*, 2007; Park *et al.*, 2008; Liu *et al.*, 2012; Goubran *et al.*, 2013; Hallack *et al.*, 2015) or photographs of an unstained brain (Bardinet *et al.*, 2002). Hallack *et al.* (2015) performed a three-stage procedure for the registration of a histology stack to an *ex-vivo* MRI dataset using feature points: (1) Matching image stack to MRI dataset, (2) rigid registration of each histological slide to MRI slice (3) and nonrigid registration. Some of the methods rely on implanting artificial markers (Humm *et al.*, 2003; Lazebnik *et al.*, 2003; Breen *et al.*, 2005) or color-coding (Alic *et al.*, 2011). Many reconstruction strategies utilize segmentation (Taylor *et al.*, 2004; Zhan *et al.*, 2007; Ou *et al.*, 2009) for volume reconstruction or for more robust similarity calculations (Ourselin *et al.*, 2001; Mosaliganti *et al.*, 2006; Seise *et al.*, 2011; Nir & Salcudean, 2013). There are also 3D reconstruction techniques based on mutual similarities between 2D histological images and known or fixed spacing between slides (Ourselin *et al.*, 2001; Arganda-Carreras *et al.*, 2010; Nir & Salcudean, 2013). The main limitation of these 3D-3D registration techniques is that they require a high number of histological sections that are not always available.

Our approach differs from the one of Hallack *et al.* (2015) in the respect that one single slide can be registered directly to the 3D dataset and that the matching surface can be curved to adapt to large deformations. In our work, we focus on a more challenging type of histology registration, namely single slide-to-volume registration (Sarve *et al.*, 2008). One of the most recent approaches by Hoerth *et al.* (2015) registered semiautomatically 2D images within 3D  $\mu$ CT data, using the generalized Hough transform. Lundin *et al.* (2017) presented an accurate approach based on binary data that requires a presegmentation step and is tailored to trabecular bone. In Wachowiak *et al.* (2004), the authors applied a global optimization for rigid 2D CT and simulated ultrasound slices (USs) to 3D histology registration. With normalized mutual information (NMI) as a cost function, the optimal parameters for particle swarm optimization were determined. Ferrante & Paragios (2013) based the registration on a grid of control points that represents both in- and out-of-plane deformation. By pairwise over-parametrization of the graphical model, they overcome inefficiency of the proposed model. The real-time registration of US slices to MRI explored by Pardasani *et al.* (2016) was able to improve the initial pose using patch-based similarity. Several methods also account for nonlinear deformations perpendicular to the slicing plane, which can often occur

in soft tissue specimens (Schormann *et al.*, 1995; Kim *et al.*, 2000; Dauguet *et al.*, 2007; Goubran *et al.*, 2015). Among nonrigid registration techniques applied to histology, one can find methods based on splines (Dauguet *et al.*, 2007; Osechinskiy & Kruggel, 2010) or on a radial basis (Goubran *et al.*, 2015) which require a selection of control points and a full multigrid approach (Schormann & Zilles, 1998). One of the attempts to incorporate nonrigid deformation was made by Osechinskiy & Kruggel (2010), who introduced a general framework for slice deformation in 3D space and implemented different techniques to identify the best-performing set of parameters. Slide-to-volume registration was also investigated by Kim *et al.* (2000), who used nonlinear polynomial functions to relate the coordinates of 2D histology to 3D MRI. Although these methods achieve reasonable results in registration, they need manual interventions at the stage of either segmentation or near ground truth initialization, where the ground truth corresponds to the best fit.

Manual detection of the histological slide in a 3D volume is a very time-consuming task and can last up to 1 day for one slide. Recently, we have developed an automatic algorithm for 2D histology to 3D  $\mu$ CT localization (Chicherova *et al.*, 2014) and showed its application on jaw bone data. Although the algorithm performed very well for most of the specimens, in some cases localization improvement was needed. In this paper, we extend the framework by registering more accurately each histological slide into the volume. We propose a combined rigid and deformable registration approach for hard and soft tissue samples. The main elements of the proposed method are NMI (Viola & Wells III, 1997; Studholme *et al.*, 1999; Pluim *et al.*, 2003) and Legendre polynomials, which are used as basis functions to approximate surface deformation. In addition to being fully automatic, the proposed method is significantly more accurate than the first approach introduced by Chicherova *et al.* (2014).

## Materials and methods

We used two datasets to evaluate the performance of the two-step optimization frameworks. The first dataset originated from a dental study about jaw bone augmentation materials (Stalder *et al.*, 2014). The bone specimens were extracted from patients directly before inserting the dental implants. The procedure was approved by the responsible Ethical Committee, study protocol number 290/13, to perform a combined histology and tomography study. Five male and four female patients, aged between 46 and 75 years, obtained treatments of bone defects at the molars in the upper and lower jaw ( $n = 8$  and  $n = 1$ , respectively). The bone graft materials used were BoneCeramic<sup>®</sup> (Institute Straumann AG, Basel, Switzerland) in one case, easy-graft<sup>™</sup> (SUNSTAR Degradable Solutions AG, Schlieren, Switzerland) in four cases and Bio-Oss<sup>®</sup> (Geistlich Biomaterials, Wolhusen,

**Table 1.** List of tomograms including specimen specifications.

#	Patient	age (Gender) [years]	Biopsy location ISO 3950	Grafting material	Dataset voxel length [ $\mu\text{m}$ ]	Dataset size [voxel]	No. of slides
1	A	70(m)	11	easy-graft <sup>TM</sup>	4.3	861×861×1939	6
2	B	74(f)	11	easy-graft <sup>TM</sup>	8.6	301×301×969	9
3	C	46(m)	23	Bio-Oss <sup>®</sup>	8.6	301×301×1093	7
4	D	47(m)	16	BoneCeramic <sup>®</sup>	8.6	421×421×753	6
5	E	57(m)	34	easy-graft <sup>TM</sup>	8.6	301×301×507	6
6	F	75(m)	16	Bio-Oss <sup>®</sup>	8.6	320×320×718	4
7	G	63(f)	15	BoneCeramic <sup>®</sup>	8.6	440×440×738	5
8	H	46(f)	21	easy-graft <sup>TM</sup>	8.6	300×300×799	6
9	I	47(f)	26	Bio-Oss <sup>®</sup>	8.6	381×381×416	4
10	E	57(m)	34	easy-graft <sup>TM</sup>	4.3	621×621×1269	5

Datasets #9 and #10 were not considered in the standard error analysis because they required an adjustment of the setup (see Section 3.1) for a successful registration.

Switzerland) in three cases (Table 1). After 5 months, the biopsy was harvested with a trephine bur 3 mm in diameter exactly at the position for implant placement. These biopsies were composed of soft tissues, existing and newly formed bone, as well as augmentation and embedding materials (Stalder *et al.*, 2014). The pathology samples were cylindrical biopsies with a diameter of around 2 mm and a length of approximately 4 mm. In order to analyze the integration of the graft in the jaw, a  $\mu\text{CT}$  of the whole specimen was acquired. The jaw biopsies were scanned using synchrotron radiation-based micro computed tomography (SR $\mu\text{CT}$ ). The measurements were performed at the beamline W2 (HASY-LAB/DESY, Hamburg, Germany, operated by HZG Research Center, Geesthacht, Germany) in conventional absorption contrast mode. The photon energy corresponded to 25 keV. The detector featured  $3056 \times 3056$  pixels (effective pixel length  $2.2 \mu\text{m}$ ), which were binned by a factor of two before reconstruction to increase the density resolution (Thurner *et al.*, 2004). The tomogram was obtained from a set of 721 equiangular radiographs along  $180^\circ$  using the standard filtered back-projection reconstruction algorithm (Stalder *et al.*, 2014). The cerebellum specimen was scanned using the CT-system nanotom<sup>®</sup> m (phoenix | X-ray, GE Sensing & Inspection Technologies GmbH, Wunstorf, Germany) in absorption contrast mode with an accelerating voltage of 60 kV and a voxel length of  $3.5 \mu\text{m}$ . The dataset was resized to a voxel length of  $7 \mu\text{m}$  using MATLAB<sup>®</sup> R2016a (The MathWorks, 135 Inc., Natick, MA, U.S.A.). Subsequently, five to nine histological cross-sections through the horizontal plane of the specimen were taken. After the SR $\mu\text{CT}$  data acquisition, the biopsies were placed in customized polytetrafluoroethylene molds and embedded with a methyl methacrylate solution consisting of methacrylate-methyl ester (Sigma-Aldrich Chemie GmbH, Buchs, Switzerland); dibutyl phthalate (Merck-Schuchardt OHG, Hohenbrunn, Germany) and Perkadox (Dr. Grogg Chemie AG, Stetten,

Switzerland) with a ratio of 89.5:10.0:0.5. After embedding, the specimens were stored and dried at room temperature. A diamond saw (Leica 1 SP 1600, Leica Instruments GmbH, Nussloch, Germany) served for cutting circularly shaped sections of the cylindrically shaped biopsies. The sections were glued (Cementit CA 12, Merz+Benteli AG, Niederwangen, Switzerland) on opal acrylic slides (Perspex GS Acrylglas Opal 1013, Wachendorf AG, Basel, Switzerland), wrapped in aluminium foil and pressed overnight under a metal block of 1 kg weight. Further, thinning down to a thickness of  $300 \mu\text{m}$  was achieved through grinding (EXACT CS400, EXACT Apparatebau, Norderstedt, Germany) and treatment with sandpaper (grit size 1200, Struers GmbH, Birmenstorf, Switzerland). Subsequently, the surfaces were polished on a Struers Planopol-V (Struers GmbH) with sandpaper (grit size 4000, Struers GmbH). The polished sections were etched with formic acid (0.7%, Sigma Aldrich) for 2 min, cleared and etched for another 2 min, rinsed with water and later surface-stained with toluidine blue (1% stock solution in 0.1 M phosphate buffer pH 8.0, Sigma Aldrich) for a duration of 10 min. The sections were digitally recorded with a microscope (Leica M420, Camera DFC 320, Leica Microsystems, Heerbrugg, Switzerland, magnification  $1.0 \times 18.6 - 22.3$ ) using the software Image Manager 1000 (Leica Microsystems) (Stalder *et al.*, 2014). The histology images were scanned with a lateral pixel length of  $1.6 \mu\text{m}$ . Before applying the registration pipeline, the images were down-sampled to approximate the voxel length of the CT data. The thickness of histological sections was limited to  $300 \mu\text{m}$  in the present study, because the biopsies were not de-calcified and contain the brittle grafting material. The slide, however, was only stained in the surface-near region in a thickness of approximately  $10 \mu\text{m}$ . Each histological slide resulted in an RGB image ranging from  $300 \times 300$  to  $861 \times 861$  pixels. The  $\mu\text{CT}$  data are 3D matrices of eight-bit gray-scale values. The data comprise a volume between  $301 \times 301 \times 507$  and  $301 \times 301 \times 1093$  voxels



with a binned isotropic voxel length of  $8.6 \mu\text{m}$ . Two datasets were recorded with a voxel length of  $4.3 \mu\text{m}$  and comprise of  $861 \times 861 \times 1939$  and  $621 \times 621 \times 1269$  voxels, respectively. Ten datasets of nine patients were included in this study (Table 1).

The second dataset corresponds to a cylindrical specimen, obtained post-mortem from the cerebellum of a 73-year-old male. The specimen was 6 mm in diameter and 4.5 mm in length. It was extracted from the donated human brain and fixed in 4% histological-grade buffered formalin. The sample was dehydrated and paraffin-embedded according to standard pathology procedures. The cylindrical sample for the tomography measurement was extracted from the paraffin block using a metal punch with an inner diameter of 6 mm. The cerebellum specimen was scanned using the CT-system nanotom<sup>®</sup> m (phoenix|X-ray, GE Sensing & Inspection Technologies GmbH) in absorption contrast mode with an accelerating voltage of 60 kV and a voxel length of  $3.5 \mu\text{m}$ . These data were then filtered with a median filter followed by an adaptive Gaussian filter in VGStudio MAX 2.0 (Volume Graphics GmbH, Heidelberg, Germany), were resized to a voxel length of  $7 \mu\text{m}$  using MATLAB<sup>®</sup> R2016a (The MathWorks, 135 Inc.), cropped and saved in 8 bit grayscale 3D matrix  $860 \times 860 \times 901$  pixels. In total, four histological slides were sectioned (thickness  $4 \mu\text{m}$ ) resulting in RGB images  $860 \times 860$  pixels in size with a resolution of about  $7 \mu\text{m}$ . To obtain the histological slides, the paraffin cylinder was re-embedded in a standard paraffin block by partial melting and the addition of fresh paraffin. Sections were cut using a microtome from the upper part of the sample, left to float on a water bath and then collected one by one and mounted on glass slides by hand. The slides were then dried out and stained with haematoxylin and eosin (H&E), following a standard protocol. Images of the resulting slides were taken at  $2\times$  optical magnification on a combined light microscope/digital camera system (Olympus DP73+Olympus BX43, Olympus Schweiz AG, Volketswil, Switzerland). All of the histological images were converted to grayscale, cropped and flipped, if needed.

Our approach for deformable 2D-3D registration consists of three main steps (Fig. 1). First, we find a matching slice to the histological image in the 3D  $\mu\text{CT}$  dataset, using our previously presented approach (Chicherova *et al.*, 2014), that matches histological slides to CT data using feature detection and matching followed by an optimal plane search based on a density-biased random sample consensus (RANSAC). Second, we rigidly register the histological image to the found slice. And lastly, starting from the initial match, we deform the plane by using an optimization framework based on NMI (see also, Table 2).

The ground truth for the counterpart of histological slide in the CT data corresponds to the registration result manually identified by four experts. The pipeline was implemented in MATLAB<sup>®</sup> R2016a (The MathWorks, 135 Inc.) for a Linux system running Ubuntu 15.10.

### Initialization

Initialization is the first step in our method that roughly localizes the histological slide in the 3D space of the  $\mu\text{CT}$  data. Histological sectioning can be represented as a plane within the 3D volume of the  $\mu\text{CT}$  dataset, defined by the plane equation  $Ax + By + Cz + D = 0$ . To find the plane coefficients, we start by computing matching points between the histology image and each image of the  $\mu\text{CT}$  data. Corresponding points between histology images and  $\mu\text{CT}$  images are found with the scale and rotation invariant feature detector Speeded Up Robust Features (SURF) (Bay *et al.*, 2008). In comparison to Scale-Invariant Feature Transform (SIFT) (Lowe, 2004) and Affine SIFT (ASIFT) (Yu & Morel, 2011), it provides either more matching points or more robust correspondences (Chicherova *et al.*, 2016). The matched keypoints for each  $\mu\text{CT}$  image are subsequently stored in a 3D matrix. We assume that the density of the points is higher in the area which corresponds best to the histological slide. Therefore, next, we solve a density problem in 3D space, using a modified RANdom SAMple Consensus (RANSAC) algorithm (Fischler & Bolles, 1981; Chicherova *et al.*, 2014). After 15 000 iterations of the modified RANSAC, estimates of the normal vector parameters for the plane that includes the most inliers are chosen. The search parameters are constrained so that only planes within a certain tilting angle  $\alpha_{\text{jaw}}$ ,  $\alpha_{\text{cereb}}$  are considered. For the complete pipeline and details of this method, we refer the reader to our previous work (Chicherova *et al.*, 2014). Herein, we just mention that in comparison to the previous method, we introduce an additional parameter, namely a filter radius. The specimen's background and borders often produce wrong correspondences, and so to remove them we crop the points by taking only those lying inside a circular region in the specimen (Chicherova, 2015). We calculate the filter radius as  $M/2.8$ , where  $M$  is the size of the square  $\mu\text{CT}$  image. Another modification is associated with the number of selected points for RANSAC fit  $P_{\text{left}}$ , which is calculated depending on the total number  $P_{\text{total}}$  of matching points:

$$P_{\text{left}} = \begin{cases} P_{\text{total}} & \text{if } P_{\text{total}} < 1500 \\ 1500 & \text{if } 1500 < P_{\text{total}} < 5000 \\ P_{\text{total}}/3 & \text{if } 5000 < P_{\text{total}} < 10000 \\ P_{\text{total}}/4 & \text{if } 10000 < P_{\text{total}} < 40000 \\ 10000 & \text{if } 40000 < P_{\text{total}} \end{cases} \quad (1)$$

These parameter values were selected empirically. The parameters for SURF<sup>1</sup> are left to default as well as for the second nearest neighbour criterion (distance ratio = 0.8). The angle between the normal to the plane and z-axis is set to  $\alpha_{\text{jaw}} = \pi/8$  and  $\alpha_{\text{cereb}} = \pi/36$  for the jawbone and the cerebellum datasets according to their pixel size. The proposed values of specific parameters are successfully applied to other X-ray based modalities as well (Chicherova, 2015; Chicherova

<sup>1</sup> [http://www.mathworks.ch/matlabcentral/fileexchange/28300-opensurfaincluding-image-warp-](http://www.mathworks.ch/matlabcentral/fileexchange/28300-opensurfaincluding-image-warp)

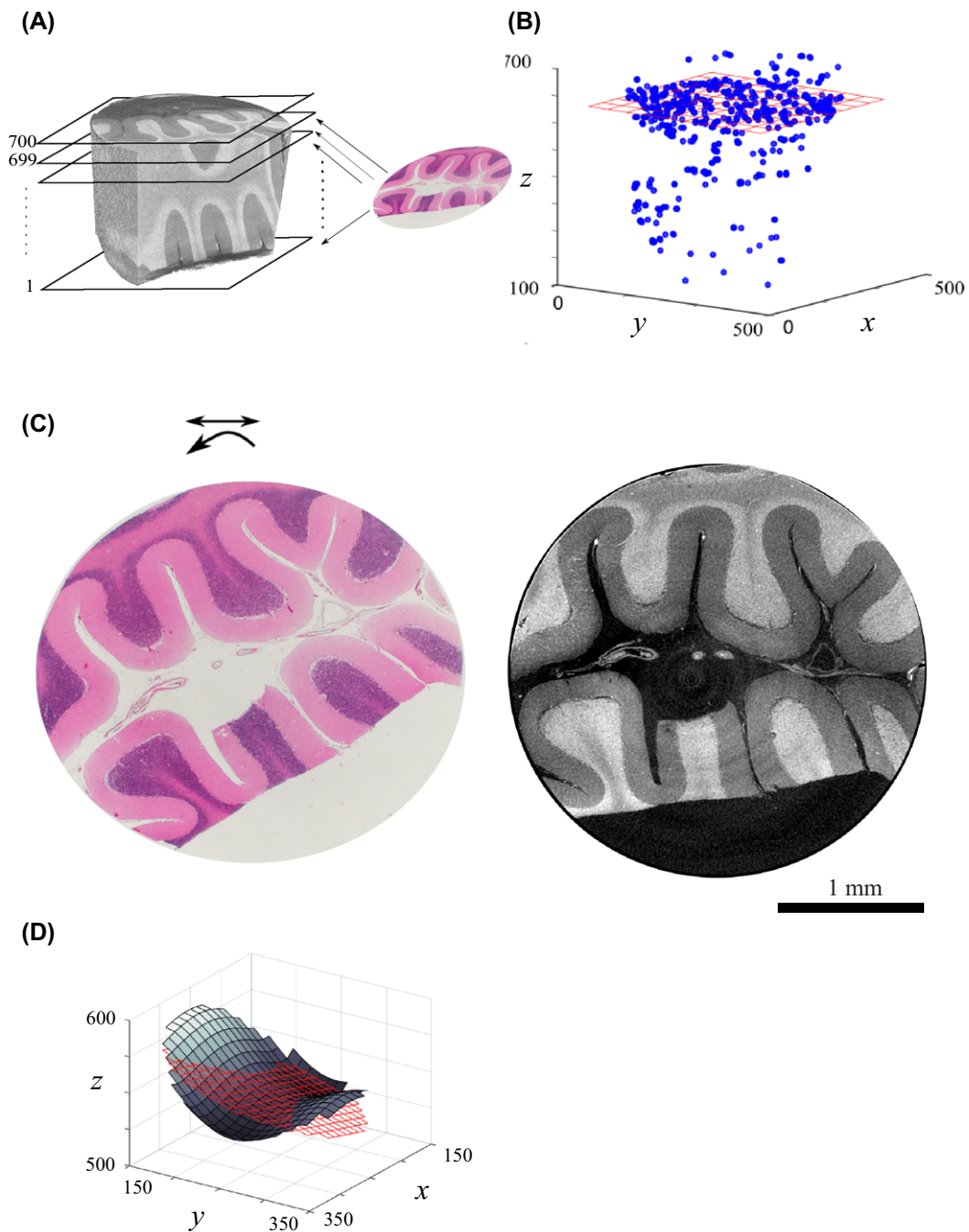


**Fig. 1.** Deformable 2D-3D registration pipeline. (A) Matching histology with every slice in the  $\mu$ CT. (B) Plane fitting to 3D keypoints cloud. (C) Affine 2D registration of histology to the matching tomogram. (D) Deformable optimization of the found plane. The voxel positions are provided in  $x$ -,  $y$ -, and  $z$ -direction.

*et al.*, 2016; Hieber *et al.*, 2016; Khimchenko *et al.*, 2016). Default parameters were applied for the built-in routines of RANSAC and the feature detection algorithms. The parameters, to be adjusted, are the maximal angle, the radius of the specimen, the number of iterations of RANSAC (10 000 by default) and the number of cloud points (10 000 by default). In

the computational experiments only, the maximal angle and the radius had to be adjusted to the specimen type. The radius is given by the geometry of the specimen. The maximal angle is estimated by the operator. For homogeneous specimens, such as the tissue of the cerebellum, a relatively small angle has to be selected to obtain reasonable results.



**Table 2.** Algorithm: deformable slide-to-volume registration.

---

Input: Histological image  $I$  and  $\mu$ CT 3D dataset  $V$ , RANSAC default parameters (threshold = 10, # iterations 10 000, # cloud points 10'000),  $\alpha_{\text{jaw}} = \pi/8$ ,  $\alpha_{\text{cereb}} = \pi/36$   
 Output: Surface coefficients  $c_{\text{optim}}$

---

1. Find matching feature points between histological slide and each image in the 3D  $\mu$ CT dataset
  2. Create a binary 3D matrix out of the  $\mu$ CT corresponding points
  3. Assign weights to each point and filter the 3D point cloud based on weights and radius
  4. Fit a plane into the filtered 3D cloud and extract matching  $\mu$ CT slice
  5. Register the histology and the  $\mu$ CT image in 2D
  6. Find coefficients  $c_0$  of the plane in Legendre bases
  7. Starting from  $c_0$ , optimize the surface coefficients  $c_{\text{optim}}$  using NMI return  $c_{\text{optim}}$
- 

### 2D-2D registration

Having obtained the plane normal vector coordinates  $n_{\text{init}}$  from the previous step, we interpolate an image out of the  $\mu$ CT dataset. In order to improve the slice position in 3D with NMI, 2D-2D registration is required. Our 2D-2D automatic registration framework is divided into two subsequent transformations, first a coarse rigid transformation and then refinement with affine registration. Let  $I(x, y)$  and  $J(x, y)$  be the histology image and the  $\mu$ CT image obtained from the initialization. Here,  $I : \Omega \subset \mathbb{R}^2 \rightarrow \mathbb{R}$  and  $J : \Omega \subset \mathbb{R}^2 \rightarrow \mathbb{R}$ . For coarse registration, we use a very efficient approach, called the RANSAC homography algorithm, which calculates the projective transformation matrix  $H$  between two images by using two sets of corresponding points. We use SURF to identify new corresponding points between the two images. Let  $\{x_n^I, y_n^I\}$ ,  $\{x_n^J, y_n^J\}$  be the matching points from the SURF algorithm, where  $n = 1, \dots, N$  and  $N$  are numbers of putative matched points in the two images. We are looking for a linear mapping between the two sets of points that will satisfy the following equation:

$$\begin{pmatrix} x_n^J \\ y_n^J \\ 1 \end{pmatrix} = \underbrace{\begin{pmatrix} h_{1,1} & h_{1,2} & h_{1,3} \\ h_{2,1} & h_{2,2} & h_{2,3} \\ h_{3,1} & h_{3,2} & h_{3,3} \end{pmatrix}}_{:=H} \begin{pmatrix} x_n^I \\ y_n^I \\ 1 \end{pmatrix}. \quad (2)$$

The RANSAC homography algorithm solves the problem by randomly picking four corresponding point pairs and calculating the transformation matrix. Then, it counts the number of inliers, i.e. points that are mapped within a certain threshold ( $t = 0.01$  voxel length), from one image to another. If the number of inliers is higher for one matrix than for the previous best one, it saves it as a possibly better homography matrix. The final matrix with the maximum number of inliers is pro-

duced after 10 000 iterations. This choice is a trade off between robustness and speed.

The main limitation of this algorithm is that it very much depends on the ratio of correctly versus wrongly matched pairs. It may produce an unrealistic transformation if the supplied points are incorrect. In some cases, the  $\mu$ CT images from the initialization look quite dissimilar from the histology, which on top of the multimodal nature of the images leads to a high number of unreliable inliers. Hence, to improve the robustness of the registration, we limit the transformation to rotation and shifting, leaving only three degrees of freedom. Thus, the transformation matrix becomes for any  $\alpha \in [0, 2\pi]$

$$\begin{pmatrix} x_n^J \\ y_n^J \\ 1 \end{pmatrix} = \begin{pmatrix} \cos \alpha & -\sin \alpha & t_1 \\ \sin \alpha & \cos \alpha & t_2 \\ 0 & 0 & 1 \end{pmatrix} \begin{pmatrix} x_n^I \\ y_n^I \\ 1 \end{pmatrix} = S \begin{pmatrix} x_n^I \\ y_n^I \\ 1 \end{pmatrix}. \quad (3)$$

For  $\vec{x}$  in the domain of image  $I$ , we define  $I_S = I \circ S^{-1}(\vec{x}) := I(S^{-1}\vec{x})$  as an output histology image after rotation and translation. To find the new transformation matrix, we integrated the Kabsch<sup>2</sup> algorithm into the RANSAC framework. As soon as the coarse rigid registration is obtained, we improve registration with an affine transformation  $T$ . The transformation matrix  $T^*$  of the image in this case is determined by maximizing NMI between the histology image  $I_S$  and the CT image  $J$ :

$$T^* = \arg \max_T \text{NMI}[I_S \circ T^{-1}, J], \quad (4)$$

where  $T$  is a matrix in the space of all the affine transformations and NMI is calculated based on images' marginal and joint entropies  $E$  as

$$\text{NMI} = \frac{E(I_S \circ T^{-1}) + E(J)}{E(I_S \circ T^{-1}, J)}. \quad (5)$$

The final image is then calculated as  $I_{AS} = I_S \circ (T^*)^{-1}$ . The optimizer follows the 'one plus one' evolution strategy (Styner *et al.*, 2000). The maximum number of iterations of the optimizer is set to 300, with an initial radius of 0.004. The number of histogram bins is calculated as the median value of the Freedman–Diaconis, Scott's and Sturges' methods.

### Deformable and rigid 2D-3D registration

After registering the histological image to the  $\mu$ CT image in 2D, we now exploit the benefit of mutual information, which is a well-known similarity measure employed for multimodal images. NMI takes into account a dense representation of the image, whereas SURF compares only sparsely distributed points. By using every pixel intensity, more sensitive registration is achieved. In an iterative optimization framework,

<sup>2</sup> <http://ch.mathworks.com/matlabcentral/fileexchange/25746-kabsch-algorithm>

we calculate NMI between the histology and an image interpolated from a deformed surface in the  $\mu$ CT volume. Surface deformations are calculated as the sum of a set of bases. With this limited set of basis functions, we approximate a function space for all possible deformations between the two modalities. As basis functions, we use associated Legendre polynomials  $P_l^m(x) = (-1)^m(1-x^2)^{m/2} \frac{d^m}{dx^m} P_l(x)$  on the interval  $-1 \leq x \leq 1$ , where  $P_l(x) = \frac{1}{2^l l!} \left[ \frac{d^l}{dx^l} (x^2-1)^l \right]$  are nonassociated Legendre polynomials,  $l \in \mathbb{Z}$  is a degree of the polynomial and  $m = 0, \dots, l$  is an order of the polynomial. Legendre polynomials are solutions to the Legendre differential equation and are spherical harmonics. The choice of Legendre polynomials is based on their orthogonality, which enables linear least squares of an independent system of equations. Furthermore, they constrain surface deformations allowing for reasonable slice transformations. However, one can choose other orthogonal polynomials as bases, depending on the deformation of the specimen. Although B-splines are a commonly used basis for nonrigid deformation, this is not a reasonable solution for our case. B-spline is a piecewise deformation model for local deformations which requires control points and consequently brings a lot of degrees of freedom. This is not only computationally demanding, but it may also lead to unrealistic deformations.

We built the Legendre basis functions on a regular grid in the 3D Cartesian coordinate system. The first basis is the Legendre polynomial of zero degree ( $l = 0$ ),  $p_1 = P_0^0$ , which is a plane parallel to the  $xy$ -plane. This basis accounts for shifting along the  $z$ -axis. The next two bases are Legendre polynomials of first degree ( $l = 1$ ),  $p_2 = P_1^0$ ,  $p_3 = P_1^1$ . The first order  $P_1^0$  ( $m = 0$ ) corresponds to an angled plane and the second order  $P_1^1$  ( $m = 1$ ) corresponds to a paraboloid. These bases account for angulation of the plane and parabolic deformation of the tissue. We enrich our bases with  $p_4 = P_2^0$ ,  $p_5 = P_2^2$ ,  $p_6 = P_4^0$ ,  $p_7 = P_4^1$ ,  $p_8 = P_5^1$  Legendre polynomials. In total, we obtain 15 bases  $P = \bigcup_{k=1}^{15} p_k$ , including the transposed ones of each basis except the first one. The initial search starts from the plane obtained from the initialization step. We represent this plane with our base functions and extract associated coefficients. Let  $F = f(x, y)$  be the plane obtained from fitting RANSAC to the matching points. To represent this function with Legendre polynomials, we sample randomly  $M$  times this plane  $F_1 = f(x_1, y_1), \dots, F_M = f(x_M, y_M)$  and obtain a vector  $\psi = [F_1, \dots, F_M]^T \in \mathbb{R}$  of  $z$  coordinates that lie on this plane. The same  $x, y$  coordinates of the sample points are then used to select  $z$ -values of the Legendre basis functions. Thus, for each basis, we obtain a vector  $\tilde{p}_k = [p_k(x_1, y_1) \dots p_k(x_M, y_M)]^T$ . Therefore, the plane can be represented in Legendre bases as  $\psi = \sum_{k=1}^{15} c_k \tilde{p}_k$ , where  $c_k \in \mathbb{R}$  are the basis coefficients.

We calculate the coefficients as a least square solution of a system of linear equations. These coefficients are then provided as arguments in an optimization framework which maximizes NMI.

**Table 3.** Median errors for the rigid NMI-based registration.

Dataset #	1	2	3	4	5	6	7	8
Tilting angle error [deg]	1.4	0.6	0.9	0.3	0.8	1.9	0.7	0.6
Distance error [ $\mu\text{m}$ ]	36	7	12	2	8	34	8	8

$$c_{\text{optim}} = \arg \max_c \text{NMI}[J(c), I_{AS}], \quad (6)$$

where  $J(c)$  is an interpolated image from a surface obtained with  $\tilde{p}_k$  basis functions. As an optimization algorithm, we use a bounded version of the Nelder–Mead simplex direct search<sup>3</sup>, which is one of the best solutions for non-smooth objective functions (Maes *et al.*, 1999; Wachowiak *et al.*, 2004). The Nelder–Mead simplex is a local optimizer that provides accurate results when the initial orientation is close to the true transformation. To increase the search space, we initialize the optimization with 20 random planes close to the initialization plane. After 20 iterations, we choose the one with the highest NMI.

In this work, we explore both rigid and nonlinear deformation models. The difference between them is the number of bases in the optimization. For rigid 2D-3D registration, we take only the three Cartesian bases  $x, y, z$ . Therefore, the rigid pipeline optimizes the normal vector coordinates to the plane  $\vec{n} = [A \ B \ C]^T$ . For nonlinearly deformable surfaces, we use the Legendre polynomials. The following constraints are used in both frameworks. The plane angle is set to  $\alpha_{\text{jaw}}$  and  $\alpha_{\text{cereb}}$  for the corresponding data, and the shift along the vertical axis is  $\pm 80$  slices. The brute force constraints lie in the same interval. We also limit the Legendre bases to exploit only feasible deformations  $[10^4, 10^4, 10^4, 5 \cdot 10^3, 10^2, 10^2]$  for the  $p_3$  until  $p_8$  correspondingly.

## Results

### Jaw bone dataset - the rigid registration framework

The rigid NMI-based registration framework was evaluated on jaw bone datasets. The histological slides in these datasets contained only limited nonrigid deformations perpendicular to the cutting plane, due to the presence of hard, bony tissue. Therefore, for these datasets, it was sufficient to perform rigid registration. To assess the performance of the framework quantitatively, we calculated the angle between the normal vector obtained with optimization and the manually found example (Table 3), which gave us an idea of how well the tilting of the plane had been determined with the method. We also computed the distance between the two planes to determine how far the found plane was from the ground truth. We calculated the distances from the origin along the  $z$ -axis for the optimized plane and the ground truth, and then we subtracted them

<sup>3</sup> <http://ch.mathworks.com/matlabcentral/fileexchange/8277-fminsearchbnd-fminsearchcon>

from each other. The median values of these errors for eight datasets are summarized in Table 3. Manual registrations were subsequently improved by four experts, which is regarded as the ground truth in this study. In addition, to evaluate the variability of the ground truth, we calculated mean standard variation of further manual registration values for four histological slides. Deviation of vertical position was seven slices and of the tilting angle was  $2^\circ$ . As the high-resolution CT data exhibit many anatomical details, the manual results were very similar to histological images (see Khimchenko (2016)).

The method accurately determined the tilting angle of the plane. Indeed, the angle error did not exceed  $1.4^\circ$ . The median distance error for the optimized rigid registration was also very low for most of the datasets. The largest errors were in the first and sixth datasets, 36 and  $34\ \mu\text{m}$ , respectively. From a visual assessment, we consider a distance error of  $60\ \mu\text{m}$  as a reasonable registration. This length corresponds to the size of the characteristic anatomical structures of the human jaw, i.e. the Haversian canals with a diameter of about  $60\ \mu\text{m}$ . Therefore, according to this assessment, our algorithm registered well 47 out of 58 histological slides. The time needed for the linear interpolation of a 2D image from a 3D volume grows as  $O(N)$ , where  $N$  is the number of voxels in the 3D datasets. We compared the computational effort of two datasets from the same patient E, where two pieces of the biopsy were processed separately. The average computational time for registering one histological slide in a volume of  $621 \times 621 \times 1269$  voxels was 26.2 min (3.6 min for SURF) compared to 2.8 min (0.3 min for SURF) in a  $301 \times 301 \times 507$  voxel dataset. Consequently, a 10 times larger volume gives rise to an increase of the computational effort by a factor of approximately nine. All the calculations were performed sequentially in MATLAB<sup>®</sup> R2016a on Ubuntu 15.10 with 64 GB of RAM and Intel<sup>®</sup> Xeon E5-2620 v3 (6 cores, 2.4 GHz/3.2 GHz Turbo).

To determine if the new pipeline had improved the initial matching, we compared the SURF-based and the rigid NMI-based pipelines with the ground truth. We calculated the tilting error and the distance error for both methods (Fig. 2).

From the comparative distance errors, one can see that in the majority of the cases, slice localization improved. Furthermore, the dispersion of the results decreased, which suggests a more stable behaviour. However, for the first dataset, there is a small deterioration. This dataset had a very high resolution, so there were several reasonable registration positions. Hence, for most of the histologies, the difference in registration between the two methods was not significant. The largest improvement was achieved in dataset #7, e.g. the distance error dropped from 251 to  $0\ \mu\text{m}$ . The method shows a general improvement for the tilting angle. The median error for the tilting angle does decrease, but there are outliers in some of the datasets. This is due to poor 2D-2D registration when the found initialization slice was far from the ground truth. Two examples of histological sections along with the registration results from both methods are shown in Figure 3. The

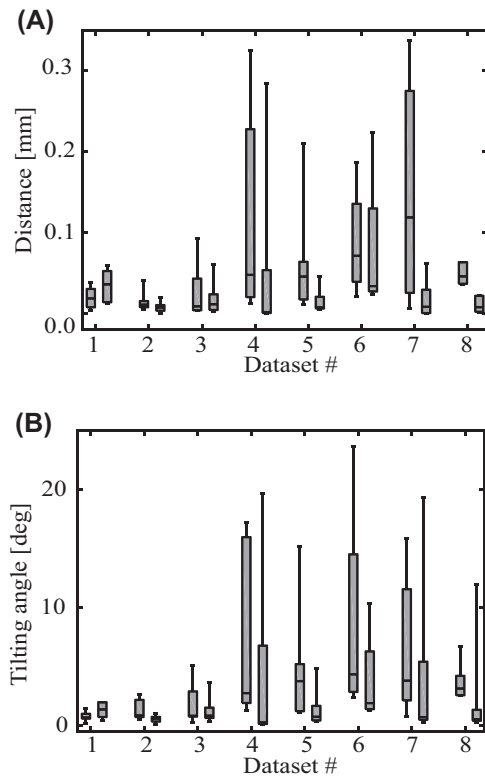


Fig. 2. Comparative error for the position (A) and the angle (B) of the plane for eight jawbone datasets. On the  $x$ -axis are shown the performance of the SURF- (left) and NMI (right)-based methods for each dataset. The median values are shown as black horizontal lines inside the boxes, 25<sup>th</sup> and 75<sup>th</sup> percentiles as bottom and top lines of the box, minimum and maximum values as bottom and top whiskers.

first method found a relevant match for the histology, but there are numerous local dissimilarities between the images. The nonparametric significance test shows that the pipeline with optimization improves registration (Kruskal–Wallis test  $p$ -value = 0.0013).

In datasets #9 and #10, the proposed method with the default setup failed to find a reasonable registration for the majority of the slides due to a large tilting angle of approximately  $20^\circ$  combined with an additional issue. For dataset #9, the registration was successful after having adjusted the contrast of the individual histological slides or a rotation of the CT data to match the histological cutting direction (Stalder *et al.*, 2014). The broken specimen of dataset #10 showed an incomplete cylindrical shape and required a rotation of the CT data or an adaptation of the filter radius for a successful registration. The illumination invariance of the SURF descriptor could not account for a 100 gray value difference. Furthermore, in one of these datasets, on top of the high tilting angle ( $22^\circ$ ), X-ray absorption values differed for the same tissue in the bottom of the specimen and on the top. This is why it was especially challenging to register this dataset and the



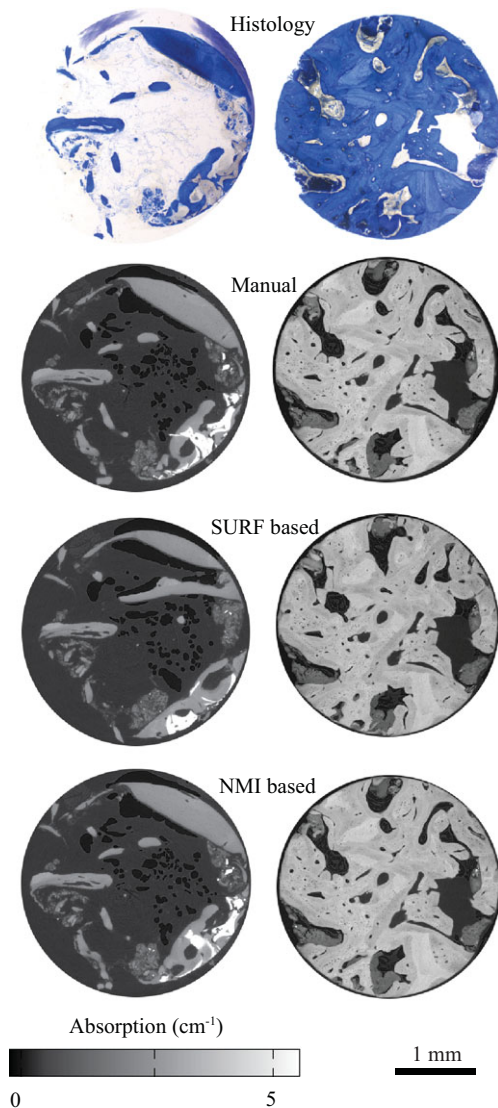


Fig. 3. Comparative slide registration for the datasets #4 (right) and #7 (left).

approach found only one reasonable registration out of four. In the dataset #2, however, the algorithm localized two histological images which were only one slice away from the ground truth. Also, the distance error for one histological slide in the dataset #8 would not fit into the boxplot region, and so it was removed for better visualization.

#### Jaw bone dataset - the deformable registration framework using simulations

Additionally, we evaluated the deformable registration framework on the jawbone datasets, using simulation. We created artificial histological slides by simulating deformed surfaces in 3D space. With these surfaces, we extracted an image from the  $\mu$ CT volume, following which we used this image as an

artificial histology section and ran it through the entire NMI-based deformable pipeline. An example of the surface and the resulting fit of the deformable pipeline for two artificial histologies is shown in Figure 4. With a color bar, we show the distance difference between the found surface and the artificial ground truth. In total, we evaluated five histological slides, and on average it took 58 min per slide. The maximum difference in the region of interest did not exceed  $50 \mu\text{m}$ .

#### Cerebellum datasets - the deformable registration framework

In contrast to the bone data, the cerebellum specimen included large non-linear deformations (Hieber *et al.*, 2016; Khimchenko *et al.*, 2016). Hence, we evaluated the deformable registration framework on this dataset. In total, four histological sections were available. The average computation time for one slide grew to 6.8 h, owing to the effort in optimization that is required to determine the deformations. In addition, the homogeneity of the tissue requires a larger number of optimization steps. For a quantitative assessment, we compared distances from the found surface to the manually found landmarks (Fig. 5). Manual registration was based on point-to-point correspondence of characteristic features such as vessels, cell groups and cracks. Then, a polynomial surface using the Matlab Curve Fitting Toolbox was fitted into the points. In three out of four histological slides, there was an improvement in registration. The median distance error improved by  $33 \mu\text{m}$  for all slides. For the histology #2, registration did not improve as the result of an image artefact. The histological section was cut from the top part of the specimen, where the tomography slices were distorted and part of the volume was removed.

Figure 6 shows an example of the first histological image and corresponding slices found with both approaches. The SURF-based method found a slice which was 0.8 mm away from the manual surface for more than half of the histology. Moreover, the deformable fit improved registration by reducing the area of high distance difference. Even though the median distance from the manual landmarks increased by  $21.6 \mu\text{m}$ , the overall registration of this histological slide improved, due to the decreased dispersion of the distances.

#### Discussion

The proposed algorithm is a coarse-to-fine registration technique that starts with the localization of a sectioning plane and finishes with the complete registration of 2D histology into the 3D space. Although hard X-ray tomography provides the 3D spatial distribution of the X-ray attenuation coefficients, the histology images exhibit the 2D spatial distribution of the stain intensity integrated perpendicular to the slide. Therefore, the contrast mechanisms are complementary. In order to exclude the impact of the contrast mechanisms, intentionally distorted CT slices were registered to the measured 3D CT data. This approach permits the error estimation excluding the impact of

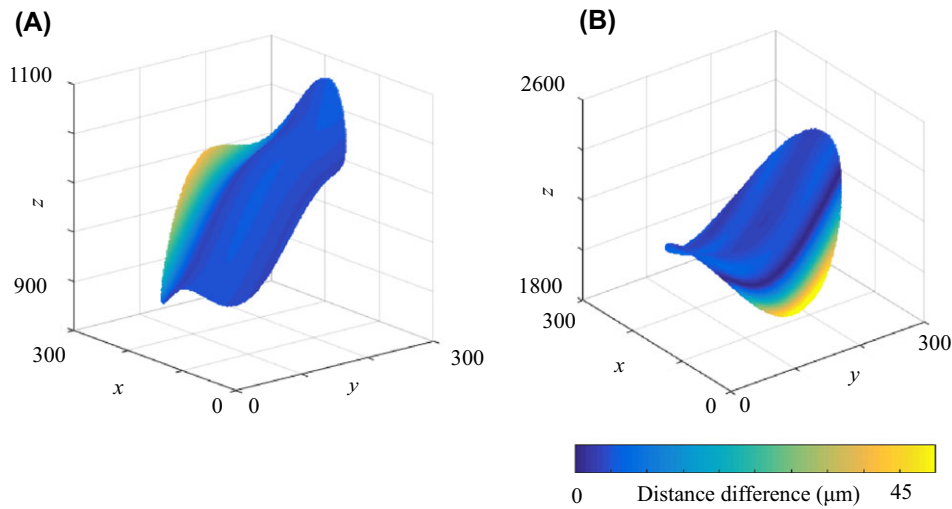


Fig. 4. Optimized fitting surfaces for the simulated histological slides colored according to the distance error from the ground truth. The voxel positions are provided in  $x$ -,  $y$ -, and  $z$ -direction.

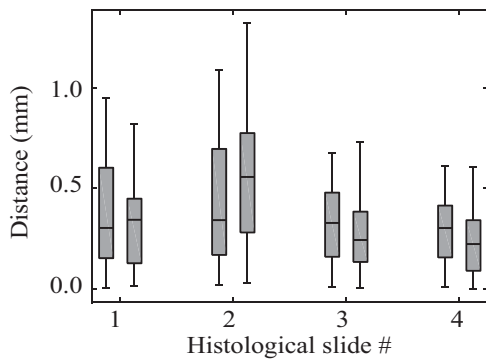


Fig. 5. Comparative distance error to the manual landmarks for four histological sections in the cerebellum dataset. On the  $x$ -axis are shown the performance of the SURF- (left) and NMI- (right) based methods for each section. The median values are shown as black horizontal lines inside the boxes, 25<sup>th</sup> and 75<sup>th</sup> percentiles as bottom and top lines of the box, minimum and maximum values as bottom and top whiskers.

the contrast mechanism and precise error can be evaluated because the ground truth is predefined. The application of the proposed method is not limited to histology to  $\mu$ CT registration – it can be applied easily to any slide-to-volume registration (Markelj *et al.*, 2012). For example, another interesting potential application is registering 2D histology to 3D MRI data (Dauguet *et al.*, 2007; Liu *et al.*, 2012; Goubran *et al.*, 2015). The important feature of our approach is that in contrast to other methods, it does not require any segmentation or other data-dependent preprocessing for images of the same size.

Overall, the method showed high accuracy in slice localization. Indeed, it allocated 47 out of 58 histological slides with high precision (distance error < 62  $\mu$ m). Furthermore, after visual inspection, we identified that eight more slices were in fact close to the ground truth position (distance

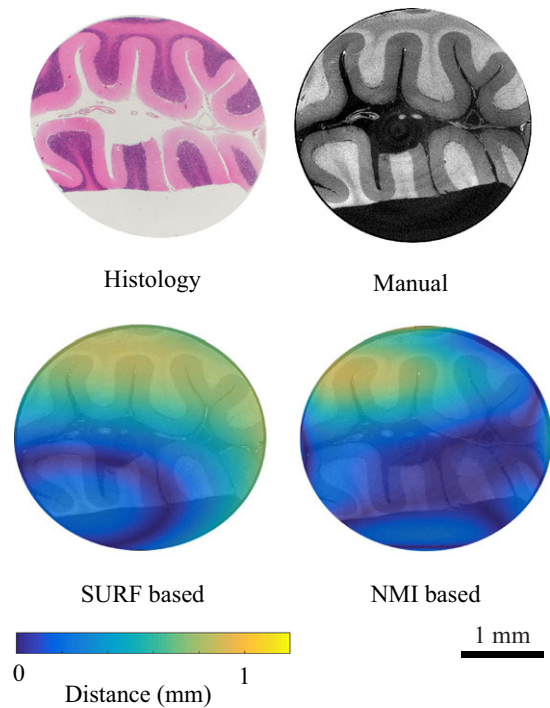


Fig. 6. Comparative slide registration for the first slide colored according to the distance error from the ground truth.

error < 1 mm). The median registration error for the 10 jaw bone volumes of 8.4  $\mu$ m is well below the slide thickness of 300  $\mu$ m and below the near-surface region that contributes to the stain intensity of the histology slide. Hence, one can conclude that the proposed procedure provides a sound registration result. The identification of the correct cutting angle correlates with the correct localization of the slide; indeed, the

improvement in the tilting angle shows a pattern similar to the distance error improvement (Fig. 2), whereas deformable registration shows high accuracy in simulations, even for highly deformed artificial slices. The distance from the ground truth surface was less than 20  $\mu\text{m}$  for the majority of the slices.

The initialization provides a plane in the 3D dataset where the most matching points are found. To accelerate the later optimization based on NMI, the histology slide should be registered rigidly to the obtained CT slice. Unfortunately, as this step relies on feature correspondences and the heuristic transformation matrix calculation, the resulting 2D-2D registration can vary for different iterations. The solution to this problem is either visual inspection or parameter optimization. However, in the majority of cases, the result of initialization is of sufficient quality and the algorithm does not need any intervention. Additional improvements to this step could be achieved with one of the multimodal histology 2D-2D registration algorithms (Jacobs *et al.*, 1999; du Bois d'Aische *et al.*, 2005; Li *et al.*, 2006; Pitiot *et al.*, 2006; Hallack *et al.*, 2015).

Another limitation of our method is that it uses the SURF algorithm for feature detection. This descriptor is built using the neighbourhood gradient around the keypoint. Hence, low-contrast images or images of mostly homogeneous tissue are likely to produce a lot of false matching points, which in turn hampers registration. One potential solution is to use another feature detector (Self-Similarity (Shechtman & Irani, 2007), ORB (Rublee *et al.*, 2011), etc.) or image preprocessing, for example, by attenuating the illumination difference between grayscale histology and  $\mu\text{CT}$  images.

Furthermore, output-matching slices after the SURF-based method can vary somewhat, depending on the parameters – sensitive parameters are the filter radius and the plane angulation constraints. For example, in dataset #4, the registration could not be achieved without radial filtering of the point cloud. With adjusted values, however, we were able to register all of the histological slides accurately.

The computation time of the algorithm is dominated by the optimization part of the method. Therefore, the method could benefit from faster 3D pixel interpolation approaches. Another possible improvement to 2D-3D optimization could be achieved by using a global optimizer such as swarm (Wachowiak *et al.*, 2004), which would make the time-consuming brute-force search unnecessary or by patch-wise registration (Ferrante & Paragios, 2013). Computational speed-up can be also attained by implementing the pipeline in C++, using parallel programming.

In conclusion, we have proposed a fully automatic approach for multi-modal 2D-3D registration which combines feature- and intensity-based approaches to accurately register a 2D slice to volume data. We have also demonstrated the high accuracy and reliability of the method and outlined potential applications beyond the particular histology- $\mu\text{CT}$  registration analyzed herein.

## Acknowledgements

The authors are very grateful to Anja Stalder and Marcel Würsch for the manual ground truth data. The authors thank Bernd Ilgenstein for the jaw biopsies and Stefan Stübinger for their histological sectioning as well as J. Hench and G. Schweighauser of the Neuropathology Department of the Basel University Hospital for providing the cerebellum sample and helping with the special preparation required for tomography measurement. Moreover, they thank the staff of the synchrotron facilities and Hans Deyhle as well as Georg Schulz for data treatment. Beamtime was granted through the project proposals I-20110780 EC and I-20110780 EC (HASYLAB at DESY, Hamburg, Germany). The work was funded by the Swiss National Science Foundation (SNSF) project 150164. Data were obtained with the support of SNSF projects 147172 and 133802.

## References

- Alic, L., Haeck, J.C., Bol, K. *et al.* (2011) Facilitating tumor functional assessment by spatially relating 3D tumor histology and *in vivo* MRI: image registration approach. *PLoS One* 6(8), e22835.
- Arganda-Carreras, I., Fernández-González, R., Muñoz-Barrutia, A. & Ortiz-De-Solorzano, C. (2010) 3D reconstruction of histological sections: application to mammary gland tissue. *Microsc. Res. Tech.* 73(11), 1019–1029.
- Bardinet, E., Ourselin, S., Dormont, D., Malandain, G., Talandé, D., Parain, K., Ayache, N. & Yelnik, J. (2002) Co-registration of histological, optical and MR data of the human brain. *In Lecture Notes in Computer Science - MICCAI 2002*, vol. 2488, pp. 548–555.
- Bay, H., Ess, A., Tuytelaars, T. & Van Gool, L. (2008) Speeded-up robust features (SURF). *Comp. Vis. Image Understand.* 110, 346–359.
- Bernhardt, R., Scharnweber, D., Müller, B., Thurner, P., Schliephake, H., Wyss, P., Beckmann, F. & Goebbels, J. (2004) Comparison of microfocus- and synchrotron X-ray tomography for the analysis of osteointegration around Ti6Al4V implants. *Eur. Cells Mater.* 7, 42–51.
- Breen, M.S., Lazechnik, R.S. & Wilson, D.L. (2005) Three-dimensional registration of magnetic resonance image data to histological sections with model-based evaluation. *Ann. Biomed. Eng.* 33(8), 1100–1112.
- Ceritoglu, C., Wang, L., Selemon, L.D., Csernansky, J.G., Miller, M.I. & Ratananather, J.T. (2010) Large deformation diffeomorphic metric mapping registration of reconstructed 3D histological section images and *in vivo* MR images. *Front. Hum. Neurosci.* 4, 1–11.
- Chicherova, N., Cattin, P., Schulz, G., Fundana, K., Müller, B. & Hieber, S.E. (2015) Automatic matching of grating-based phase tomography dataset with histology. *Eur. Cells Mater.* 30(Suppl. 1), 34.
- Chicherova, N., Fundana, K., Müller, B. & Cattin, P.C. (2014) Histology to  $\mu\text{CT}$  data matching using landmarks and a density biased RANSAC. *In Lecture Notes in Computer Science - MICCAI 2014*, vol. 8673, pp. 243–250.
- Chicherova, N., Hieber, S.E., Schulz, G., Khimchenko, A., Bikis, C., Cattin, P.C. & Müller, B. (2016) Automatic histology registration in application to X-ray modalities. *Proc. SPIE* 9967, 996708.
- Dauguet, J., Delzescaux, T., Condé, F., Mangin, J.-F., Ayache, N., Hantraye, P. & Frouin, V. (2007) Three-dimensional reconstruction of stained



- histological slices and 3D non-linear registration with *in-vivo* MRI for whole baboon brain. *J. Neurosci. Methods* **164**(1), 191–204.
- du Bois d'Aische, A., De Craene, M., Geets, X., Gregoire, V., Macq, B. & Warfield, S.K. (2005) Efficient multi-modal dense field non-rigid registration: alignment of histological and section images. *Med. Image Anal.* **9**(6), 538–546.
- Ferrante, E. & Paragios, N. (2013) Non-rigid 2D-3D medical image registration using Markov random fields. In *Lecture Notes in Computer Science - MICCAI 2013*, vol. 8151, pp. 163–170.
- Ferrante, E. & Paragios, N. (2017) Slice-to-volume medical image registration: a survey. *Med. Image Anal.* **39**, 101–123.
- Fischler, M.A. & Bolles, R.C. (1981) Random sample consensus: a paradigm for model fitting with applications to image analysis and automated cartography. *Commun. ACM* **24**, 381–395.
- Germann, M., Morel, A., Beckmann, F., Andronache, A., Jeanmond, D. & Müller, B. (2008) Strain fields in histological slices of brain tissue determined by synchrotron radiation-based micro computed tomography. *J. Neurosci. Methods* **170**, 149–155.
- Goubran, M., Crukley, C., de Ribaupierre, S., Peters, T.M. & Khan, A.R. (2013) Image registration of *ex-vivo* MRI to sparsely sectioned histology of hippocampal and neocortical temporal lobe specimens. *Neuroimage* **83**, 770–781.
- Goubran, M., de Ribaupierre, S., Hammond, R.R., Currie, C., Burneo, J.G., Parrent, A.G., Peters, T.M. & Khan, A.R. (2015) Registration of *in-vivo* to *ex-vivo* MRI of surgically resected specimens: a pipeline for histology to *in-vivo* registration. *J. Neurosci. Methods* **241**, 53–65.
- Hallack, A., Papież, B.W., Wilson, J., Wang, L.M., Maughan, T., Gooding, M.J. & Schnabel, J.A. (2015) Correlating tumour histology and *ex vivo* MRI using dense modality-independent patch-based descriptors. In *Lecture Notes in Computer Science*, vol. 9467, pp. 137–145.
- Hieber, S.E., Bikis, C., Khimchenko, A., Schweighauser, G., Chicherova, N., Schulz, G. & Müller, B. (2016) Tomographic brain imaging with nucleolar detail and automatic cell counting. *Sci. Rep.* **6**, 32156–32167.
- Hoerth, R.M., Baum, D., Knötel, D. *et al.* (2015) Registering 2D and 3D imaging data of bone during healing. *Connect. Tissue Res.* **56**(2), 133–143.
- Humm, J., Ballon, D., Hu, Y. *et al.* (2003) A stereotactic method for the three-dimensional registration of multi-modality biologic images in animals: NMR, PET, histology, and autoradiography. *Med. Phys.* **30**(9), 2303–2314.
- Jacobs, M.A., Windham, J.P., Soltanian-Zadeh, H., Peck, D.J. & Knight, R.A. (1999) Registration and warping of magnetic resonance images to histological sections. *Med. Phys.* **26**(8), 1568–1578.
- Khimchenko, A. (2016) Manual landmarks selection in the cerebellum dataset [last visited January 2, 2018]. URL: <https://www.youtube.com/watch?v=TwfeiXfgZDM>.
- Khimchenko, A., Deyhle, H., Schulz, G. *et al.* (2016) Extending two-dimensional histology into the third dimension through conventional micro computed tomography. *Neuroimage* **139**, 26–36.
- Kim, B., Boes, J.L., Frey, K.A. & Meyer, C.R. (1997) Mutual information for automated unwarping of rat brain autoradiographs. *Neuroimage* **5**(1), 31–40.
- Kim, T.-S., Singh, M., Sungkara, W., Zarow, C. & Chui, H. (2000) Automatic registration of postmortem brain slices to MRI reference volume. *IEEE Trans. Nucl. Sci.* **47**(4), 1607–1613.
- Krauth, A., Blanc, R., Poveda, A., Jeanmonod, D., Morel, A. & Székely, G. (2010) A mean three-dimensional atlas of the human thalamus: generation from multiple histological data. *Neuroimage* **49**(3), 2053–2062.
- Lazebnik, R.S., Lancaster, T.L., Breen, M.S., Lewin, J.S. & Wilson, D.L. (2003) Volume registration using needle paths and point landmarks for evaluation of interventional MRI treatments. *IEEE Trans. Med. Imag.* **22**(5), 653–660.
- Li, G., Nikolova, S. & Bartha, R. (2006) Registration of *in vivo* magnetic resonance T1-weighted brain images to triphenyltetrazolium chloride stained sections in small animals. *J. Neurosci. Methods* **156**(1), 368–375.
- Liu, Y., Sajja, B.R., Uberti, M.G., Gendelman, H.E., Kielian, T. & Boska, M.D. (2012) Landmark optimization using local curvature for point-based nonlinear rodent brain image registration. *J. Biomed. Imaging* **2012**, 1.
- Lowe, D.G. (2004) Distinctive image features from scale-invariant keypoints. *Int. J. Comp. Vis.* **60**, 91–110.
- Lundin, E.L., Stauber, M., Papageorgiou, P., Ehrbar, M., Ghayor, C., Weber, F.E., Tanner, C. & Goksel, O. (2017) Automatic registration of 2D histological sections to 3D microCT volumes: trabecular bone. *Bone* **105**, 173–183.
- Maes, F., Vandermeulen, D. & Suetens, P. (1999) Comparative evaluation of multiresolution optimization strategies for multimodality image registration by maximization of mutual information. *Med. Image Anal.* **3**(4), 373–386.
- Markelj, P., Tomaževič, D., Likar, B. & Pernuš, F. (2012) A review of 3D/2D registration methods for image-guided interventions. *Med. Image Anal.* **16**(3), 642–661.
- Meyer, C.R., Moffat, B.A., Kuszpit, K., Bland, P.L., Chenevert, T., Rehemtulla, A. & Ross, B. (2006) A methodology for registration of a histological slide and *in vivo* MRI volume based on optimizing mutual information. *Mol. Imaging* **5**(1), 16–23.
- Mosaliganti, K., Pan, T., Sharp, R. *et al.* (2006) Registration and 3D visualization of large microscopy images. *Proc. SPIE* **6144**, 61442V.
- Müller, B., Deyhle, H., Lang, S., Schulz, G., Bormann, T., Fierz, F.C. & Hieber, S.E. (2012) Three-dimensional registration of tomography data for quantification in biomaterials science. *Int. J. Mater. Res.* **103**(2), 242–249.
- Nir, G. & Salcudean, S.E. (2013) Registration of whole-mount histology and tomography of the prostate using particle filtering. *Proc. SPIE* **8676**, 86760E.
- Osechinskiy, S. & Kruggel, F. (2010) Slice-to-volume nonrigid registration of histological sections to MR images of the human brain. *Anat. Res. Int.* **287860**, 1–7.
- Ou, Y., Shen, D., Feldman, M., Tomaszewski, J. & Davatzikos, C. (2009) Non-rigid registration between histological and MR images of the prostate: a joint segmentation and registration framework. In *IEEE Computer Vision and Pattern Recognition Workshops*, pp. 125–132.
- Ourselin, S., Bardenet, E., Dormont, D. *et al.* (2001) Fusion of histological sections and MR images: towards the construction of an atlas of the human basal ganglia. In *Lecture Notes of Computer Science - MICCAI 2001*, vol. 2208, pp. 743–751.
- Pardasani, U., Baxter, J.S., Peters, T.M. & Khan, A.R. (2016) Single slice US-MRI registration for neurosurgical MRI-guided US. *Proc. SPIE* **9786**, 97862D.
- Park, H., Piert, M.R., Khan, A., Shah, R., Hussain, H., Siddiqui, J., Chenevert, T.L. & Meyer, C.R. (2008) Registration methodology for histological sections and *in vivo* imaging of human prostate. *Acad. Radiol.* **15**(8), 1027–1039.
- Particelli, F., Mecozzi, L., Beraudi, A., Montesi, M., Baruffaldi, F. & Viceconti, M. (2012) A comparison between micro-CT and histology for the evaluation of cortical bone: effect of polymethylmethacrylate embedding on structural parameters. *J. Microsc.* **245**(3), 302–310.

- Pitiot, A., Bardinet, E., Thompson, P.M. & Malandain, G. (2006) Piecewise affine registration of biological images for volume reconstruction. *Med. Image Anal.* **10**, 465–483.
- Pluim, J.P., Maintz, J.A., Viergever, M. *et al.* (2003) Mutual-information-based registration of medical images: a survey. *IEEE Trans. Med. Imaging* **22**(8), 986–1004.
- Ruble, E., Rabaud, V., Konolige, K. & Bradski, G. (2011) ORB: an efficient alternative to SIFT or SURF. In *IEEE International Conference on Computer Vision (ICCV 2011)*, pp. 2564–2571.
- Sarve, H., Lindblad, J. & Johansson, C.B. (2008) Registration of 2D histological images of bone implants with 3D SR $\mu$ CT volumes. *Adv. Vis. Comput.* **5358**, 1071–1080.
- Schormann, T., Dabringhaus, A. & Zilles, K. (1995) Statistics of deformations in histology and application to improved alignment with MRI. *IEEE Trans. Med. Imaging* **14**(1), 25–35.
- Schormann, T. & Zilles, K. (1998) Three-dimensional linear and nonlinear transformations: an integration of light microscopical and MRI data. *Hum. Brain Mapp.* **6**(5–6), 339–347.
- Schulz, G., Crooijmans, H., Germann, M., Scheffler, K., Müller-Gerbl, M., Bikis, C. & Müller, B. (2011) Three-dimensional strain fields in human brain resulting from formalin fixation. *J. Neurosci. Methods* **202**, 17–27.
- Schulz, G., Waschki, C., Pfeiffer, F., Zanette, I., Weitkamp, T., David, C. & Müller, B. (2012) Multimodal imaging of human cerebellum—merging X-ray phase microtomography, magnetic resonance microscopy and histology. *Sci. Rep.* **2**, 826–833.
- Seise, M., Alhonnoro, T., Kolesnik, M. *et al.* (2011) Interactive registration of 2D histology and 3D CT data for assessment of radiofrequency ablation treatment. *J. Pathol. Inform.* **2**(2), 9.
- Shechtman, E. & Irani, M. (2007) Matching local self-similarities across images and videos. In *IEEE Conference on Computer Vision and Pattern Recognition (CVPR 2007)*, pp. 18–23.
- Stalder, A.K., Ilgenstein, B., Chicherova, N., Deyhle, H., Beckmann, F., Müller, B. & Hieber, S.E. (2014) Combined use of micro computed tomography and histology to evaluate the regenerative capacity of bone grafting materials. *Int. J. Mater. Res.* **105**(7), 679–691.
- Studholme, C., Hill, D.L. & Hawkes, D.J. (1999) An overlap invariant entropy measure of 3D medical image alignment. *Pattern Recognit.* **32**(1), 71–86.
- Styner, M., Brechbühler, C., Székely, G. & Gerig, G. (2000) Parametric estimate of intensity inhomogeneities applied to MRI. *IEEE Trans. Med. Imaging* **19**(3), 153–165.
- Taylor, L.S., Porter, B.C., Nadasdy, G. *et al.* (2004) Three-dimensional registration of prostate images from histology and ultrasound. *Ultrasound Med. Biol.* **30**(2), 161–168.
- Thurner, P., Beckmann, F. & Müller, B. (2004) An optimization procedure for spatial and density resolution in hard X-ray micro computed tomography. *Nucl. Instr. Meth. Phys. Res. B* **225**, 599–603.
- Tsai, C.-L., Lister, J., Björnsson, C., Smith, K., Shain, W., Barnes, S.C. & Roysam, B. (2011) Robust, globally consistent and fully automatic multi-image registration and montage synthesis for 3-D multi-channel images. *J. Microsc.* **243**(2), 154–171.
- Tsai, C.-L., Warger II, W., Laevsky, G. & Dimarzio, C. (2008) Alignment with sub-pixel accuracy for images of multi-modality microscopes using automatic calibration. *J. Microsc.* **232**(1), 164–176.
- Viola, P. & Wells III, W.M. (1997) Alignment by maximization of mutual information. *Int. J. Comp. Vis.* **24**(2), 137–154.
- Wachowiak, M.P., Smolíková, R., Zheng, Y., Zurada, J.M. & Elmaghraby, A.S. (2004) An approach to multimodal biomedical image registration utilizing particle swarm optimization. *IEEE Trans. Evol. Comput.* **8**(3), 289–301.
- Yu, G. & Morel, J. (2011) ASIFT: an algorithm for fully affine invariant comparison. *Image Process. On Line* **1**, 11–38.
- Zhan, Y., Ou, Y., Feldman, M., Tomaszewski, J., Davatzikos, C. & Shen, D. (2007) Registering histologic and MR images of prostate for image-based cancer detection. *Acad. Radiol.* **14**(11), 1367–1381.



### 3.3 Automatic 2D-3D Registration of Histology, MRI and CT Data

Natalia Chicherova, Simone E. Hieber, Benedikt Bitterli, Georg Schulz, Philippe C. Cattin,  
Bert Müller

The manuscript presented in this chapter presents two pipelines evaluations. First, we evaluated the limitations of the 2D-3D slice-to-volume registration technique. And second, we registered a histological slide to the MRI data through CT volume. Both pipelines exploit a known transformation of the a-priori registered MRI and CT data. Moreover, we introduced an extension of a self-similarity feature detector to explore the potential improvement of the initial slide localization step.

**Authors contribution.** Natalia Chicherova contributed to the algorithm development, its implementation, data analysis and wrote the main parts of the manuscript. Dr. Simone E. Hieber contributed to the data analysis, figures design and manuscript writing. Benedikt Bitterli contributed to the algorithm development. Dr. Georg Schulz provided the data and contributed to the data analysis. Prof. Philippe C. Cattin contributed to the algorithm development, figure design and the manuscript writing. Prof. Bert Müller initiated the project, provided the data and contributed to the manuscript writing. All the authors reviewed the manuscript.

# Automatic 2D-3D Registration of Histology, MRI and CT data

NATALIA CHICHEROVA,<sup>1,2</sup> SIMONE E. HIEBER,<sup>1,\*</sup> BENEDIKT BITTERLI,<sup>2</sup> GEORG SCHULZ,<sup>1</sup> PHILIPPE C. CATTIN,<sup>2</sup> AND BERT MÜLLER<sup>1</sup>

<sup>1</sup> Biomaterials Science Center, Department of Biomedical Engineering, University of Basel, Gewerbestrasse 14, 4123 Allschwil, Switzerland

<sup>2</sup> Center for medical Image Analysis & Navigation, Department of Biomedical Engineering, University of Basel, Gewerbestrasse 14, 4123 Allschwil, Switzerland

\*simone.hieber@unibas.ch

**Abstract:** Multimodal imaging of tissue can be used for validation purposes or provide more information than one modality alone. Multimodal tissue evaluation requires a mapping between the images in two or three dimensions. In particular, the task of registering a histological slide to magnetic resonance imaging (MRI) data is challenging because of numerous imaging artifacts including inconsistent contrast and is mostly performed manually. Here, we present a methodology to register a fractured histological slide to MRI volume data of a human cerebellum specimen. The location of matching slice is first found in a computed tomography (CT) volume data set of the same specimen that transferred to the MRI data via 3D-3D registration. Here, we propose the usage of an extension of the Self-similarity feature detector  $SL_1$ , which combines rotation invariant feature extraction and  $L_1$ -norm outlier rejection. We show that the consideration of both  $SL_1$  and SURF features leads to an improvement in the registration. The performance of the proposed registration frameworks is evaluated using the a-priori 3D registered MRI and CT data as a ground truth to exclude manual bias.

© 2018 Optical Society of America

OCIS codes: (000.0000) General; (000.2700) General science.

## References and links

1. J. P. Plum, J. A. Maintz, M. Viergever *et al.*, "Mutual-information-based registration of medical images: a survey," *IEEE Transactions on Medical Imaging* **22**, 986–1004 (2003).
2. D. L. Hill, P. G. Batchelor, M. Holden, and D. J. Hawkes, "Medical image registration," *Physics in Medicine and Biology* **46**, R1 (2001).
3. C. Studholme, D. L. Hill, and D. J. Hawkes, "Automated 3D registration of truncated MR and CT images of the head," in "Proceedings of the British conference on Machine vision," (1995), pp. 1–10.
4. F. Maes, A. Collignon, D. Vandermeulen, G. Marchal, and P. Suetens, "Multimodality image registration by maximization of mutual information," *IEEE Transactions on Medical Imaging* **16**, 187–198 (1997).
5. C. Studholme, D. L. Hill, and D. J. Hawkes, "Multiresolution voxel similarity measures for MR-PET registration," *Information processing in medical imaging* **3**, 287–298 (1995).
6. T. L. Faber, R. W. McColl, R. M. Opperman, J. R. Corbett, and R. M. Peshock, "Spatial and temporal registration of cardiac SPECT and MR images: methods and evaluation," *Radiology* **179**, 857–861 (1991).
7. E. Ask, O. Enqvist, L. Svärm, F. Kahl, and G. Lippolis, "Tractable and reliable registration of 2D point sets," in "Computer Vision–ECCV 2014," (Springer, 2014), pp. 393–406.
8. J. Kybic and M. Unser, "Fast parametric elastic image registration," *IEEE Transactions on Image Processing* **12**, 1427–1442 (2003).
9. A. Andronache, P. Cattin, and G. Székely, "Adaptive subdivision for hierarchical non-rigid registration of multi-modal images using mutual information," *Lecture Notes in Computer Science- MICCAI 2005* **3750**, 976–983 (2005).
10. M. P. Heinrich, M. Jenkinson, M. Bhushan, T. Matin, F. V. Gleeson, M. Brady, and J. A. Schnabel, "Mind: Modality independent neighbourhood descriptor for multi-modal deformable registration," *Medical Image Analysis* **16**, 1423–1435 (2012).
11. P. Markelj, D. Tomaževič, B. Likar, and F. Pernuš, "A review of 3D/2D registration methods for image-guided interventions," *Medical Image Analysis* **16**, 642–661 (2012).
12. P. De Bruin, B. Kaptein, B. Stoel, J. Reiber, P. Rozing, and E. Valstar, "Image-based RSA: Roentgen stereophotogrammetric analysis based on 2D–3D image registration," *Journal of Biomechanics* **41**, 155–164 (2008).

13. D. Zikic, M. Groher, A. Khamene, and N. Navab, "Deformable registration of 3D vessel structures to a single projection image," in "Medical Imaging," (International Society for Optics and Photonics, 2008), pp. 691412–691412.
14. S. Aouadi and L. Sarry, "Accurate and precise 2D–3D registration based on x-ray intensity," *Computer Vision and Image Understanding* **110**, 134–151 (2008).
15. S. Benameur, M. Mignotte, S. Parent, H. Labelle, W. Skalli, and J. de Guise, "3D/2D registration and segmentation of scoliotic vertebrae using statistical models," *Computerized Medical Imaging and Graphics* **27**, 321–337 (2003).
16. B. Fei, J. L. Duerk, D. T. Boll, J. S. Lewin, and D. L. Wilson, "Slice-to-volume registration and its potential application to interventional MRI-guided radio-frequency thermal ablation of prostate cancer," *IEEE Transactions on Medical Imaging* **22**, 515–525 (2003).
17. E. Bullitt, A. Liu, S. R. Aylward, C. Coffey, J. Stone, S. K. Mukherji, K. E. Muller, and S. M. Pizer, "Registration of 3D cerebral vessels with 2D digital angiograms: Clinical evaluation," *Academic Radiology* **6**, 539–546 (1999).
18. L. Frühwald, J. Kettenbach, M. Figl, J. Hummel, H. Bergmann, and W. Birkfellner, "A comparative study on manual and automatic slice-to-volume registration of CT images," *European Radiology* **19**, 2647–2653 (2009).
19. S. De Buck, F. Maes, J. Ector, J. Bogaert, S. Dymarkowski, H. Heidbüchel, and P. Suetens, "An augmented reality system for patient-specific guidance of cardiac catheter ablation procedures," *IEEE Transactions on Medical Imaging* **24**, 1512–1524 (2005).
20. E. B. De Kraats, G. P. Penney, D. Tomažević, T. Van Walsum, and W. J. Niessen, "Standardized evaluation methodology for 2-D - 3-D registration," *IEEE Transactions on Medical Imaging* **24**, 1177–1189 (2005).
21. A. Hallack, B. W. Papież, J. Wilson, L. M. Wang, T. Maughan, M. J. Gooding, and J. A. Schnabel, "Correlating tumour histology and *ex vivo* MRI using dense modality-independent patch-based descriptors," *Lecture Notes in Computer Science* **9467**, 137–145 (2015).
22. N. Chicherova, K. Fundana, B. Müller, and P. C. Cattin, "Histology to  $\mu$ CT data matching using landmarks and a density biased ransac," *Lecture Notes in Computer Science - MICCAI 2014* **8673**, 243–250 (2014).
23. S. E. Hieber, C. Bikis, A. Khimchenko, G. Schweighauser, N. Chicherova, G. Schulz, and B. Müller, "Tomographic brain imaging with nucleolar detail and automatic cell counting," *Scientific Reports* **6**, 32156–32167 (2016).
24. J. Huang, S. You, and J. Zhao, "Multimodal image matching using self similarity," *IEEE Applied Imagery Pattern Recognition Workshop (AIPR)* pp. 1–6 (2011).
25. A. Sedaghat and H. Ebadi, "Distinctive order based self-similarity descriptor for multi-sensor remote sensing image matching," *ISPRS Journal of Photogrammetry and Remote Sensing* **108**, 62–71 (2015).
26. H. Bay, A. Ess, T. Tuytelaars, and L. Van Gool, "Speeded-up robust features (SURF)," *Computer Vision and Image Understanding* **110**, 346–359 (2008).
27. K. Chatfield, J. Philbin, and A. Zisserman, "Efficient retrieval of deformable shape classes using local self-similarities," in "IEEE 12th International Conference on Computer Vision Workshops (ICCV Workshops 2009)," (IEEE, 2009), pp. 264–271.
28. G. Schulz, T. Weitkamp, I. Zanette, F. Pfeiffer, F. Beckmann, C. David, S. Rutishauser, E. Reznikova, and B. Müller, "High-resolution tomographic imaging of a human cerebellum: comparison of absorption and grating-based phase contrast," *Journal of The Royal Society Interface* pp. 1665–1676 (2010).
29. G. Schulz, C. Waschki, F. Pfeiffer, I. Zanette, T. Weitkamp, C. David, and B. Müller, "Multimodal imaging of human cerebellum-merging X-ray phase microtomography, magnetic resonance microscopy and histology," *Scientific Reports* **2**, 826–833 (2012).
30. M. N. Ahmed, S. M. Yamany, N. Mohamed, A. A. Farag, and T. Moriarty, "A modified fuzzy c-means algorithm for bias field estimation and segmentation of MRI data," *IEEE Transactions on Medical Imaging* **21**, 193–199 (2002).
31. A. Morel, *Stereotactic Atlas of the Human Thalamus and Basal Ganglia* (CRC Press, Informa Healthcare, New York, 2007).
32. M. A. Fischler and R. C. Bolles, "Random sample consensus: a paradigm for model fitting with applications to image analysis and automated cartography," *Communications of the ACM* **24**, 381–395 (1981).
33. D. G. Lowe, "Distinctive image features from scale-invariant keypoints," *International Journal of Computer Vision* **60**, 91–110 (2004).
34. N. Chicherova, P. Cattin, G. Schulz, K. Fundana, B. Müller, and S. E. Hieber, "Automatic matching of grating-based phase tomography dataset with histology," *European Cells and Materials* **30**, 34 (2015).
35. N. Otsu, "A threshold selection method from gray-level histograms," *Automatica* **11**, 23–27 (1975).
36. P. Viola and W. M. Wells III, "Alignment by maximization of mutual information," *International Journal of Computer Vision* **24**, 137–154 (1997).
37. J. Lewis, "Fast normalized cross-correlation," *Vision interface* **10**, 120–123 (1995).
38. E. Shechtman and M. Irani, "Matching local self-similarities across images and videos," in "IEEE Conference on Computer Vision and Pattern Recognition (CVPR 2007)," (2007), pp. 18–23.
39. O. Tange *et al.*, "Gnu parallel-the command-line power tool," *The USENIX Magazine* **36**, 42–47 (2011).
40. J. A. Schnabel, C. Tanner, A. D. C. Smith, D. L. Hill, D. J. Hawkes, M. O. Leach, C. Hayes, A. Degenhard, and R. Hose, "Validation of non-rigid registration using finite element methods," *Information Processing in Medical Imaging* pp. 344–357 (2001).
41. N. Chicherova, S. E. Hieber, G. Schulz, A. Khimchenko, C. Bikis, P. C. Cattin, and B. Müller, "Automatic histology registration in application to X-ray modalities," *Proc. SPIE* **9967**, 996708 (2016).
42. T. F. Cootes, C. J. Taylor, D. H. Cooper, and J. Graham, "Active shape models-their training and application,"

## Introduction

Combining two or more imaging modalities can be beneficial; for example, microscopy images can show functional information which can differentiate, say, cancer from healthy tissue. X-ray tomography is indispensable for hard tissue visualisation, whereas magnetic resonance imaging (MRI) is a perfect choice for *in vivo* brain tissue imaging. Very often, to make an accurate diagnosis, two or more imaging modalities are needed. The first important step in multi-modal image analysis is to transform images into the same coordinate system, i.e. to establish a pixel-by-pixel correspondence between the images.

Extensive research has been done on multi-modal 2 dimensional (2D) - 2D and 3 dimensional (3D)-3D data registration [1, 2], such as the numerous algorithms available for MR and computed tomography (CT) volume registration [3, 4], MRI and positron emission tomography (PET) or single photon emission computerised tomography (SPECT) [5, 6]. 2D-2D registration techniques vary from rigid (rotation and translation) corrections [7] to non-rigid approaches [8–10].

The majority of previously developed algorithms focus on 2D-2D and 3D-3D registration because usually one needs to keep the degrees of freedom reasonably small. However, several modalities exist only in 2D space, such as brightfield microscopy images, and others only in 3D. Registration in this case is still very beneficial for analysis. One 2D-3D example of registration comes from image-guided therapy, whereby the data of a patient before and during intervention should be directed to the same coordinates for better guidance [11]. Pre-interventional data are 3D CT or MRI volumes, and intra-interventional are fluoroscopy, ultrasound (US) or optical 2D images.

Almost every paper that has researched 2D-3D registration usually deals with the registration of 2D fluoroscopy projections to 3D CT data [12–14]. Fluoroscopy projections can provide spatial information about a volume as well as correspondence between coordinate systems. Most of the registration methods in this category can be reduced to contour or surface distance minimisation [15]. Several studies have investigated 2D slice to 3D volume registration, or so-called slice-to-volume registration [16–18], among which only a few have developed approaches to multi-modal registration [17, 19, 20]. Nonetheless, these methods rely on expert visual matching [17, 19] or slice pose initialisation [20].

Single CT slice-to-MRI volume registration was also explored in [7], in which the authors developed an algorithm that searched for the best matching slice in 3D by calculating the number of corresponding feature points. This method, though, can only compensate for translation in 3D space and does not allow for tilting of the slice. Another type of 2D-3D registration is concerned with histological slide-to-3D volume registration. These approaches, however, rely to a great extent on manual corrections and cannot be considered as fully automatic. Hallack et al. [21] performed a registration of histological slides to an ex-vivo MRI data set, but the procedure requires the matching of several slides in a stack as a first step. It follows a rigid and nonrigid registration of each histological slide.

In a recent article [22], we developed an algorithm which localises histological slides in a  $\mu$ CT volume data in jawbone samples, i.e. a slide-to-volume registration. The main advantage of the method is that it is fully automatic and can localise tilted slides in 3D space. The median translation error for 81% of the sections was 8.4  $\mu$ m, i.e. less than 0.002% of the sample size. In this study, we sought to extend its application to other modalities, and present the registration of a single histological slide to a 3D MRI data set via a  $\mu$ CT data set and single-slice CT to MRI data. Another motivation was that in both of the studies registration accuracy was analysed by comparing automatic results with manually found slice positions. As manual identification of correct position can be prone to errors and might change from expert to expert, we decided to

validate the framework against two previously registered MRI and CT volumes.

In this work, we also investigated a potential improvement in the framework, by designing a feature detector pipeline – more suitable for multi-modal matching – as a competitive alternative to the original feature detector. In our recent study, N. Khalili proposed employing a self-similarity descriptor (*SS*) [?], which has been already successfully applied for 2D-3D registration [23]. Moreover, we exploited rotation invariant *SS* descriptors studied in the literature [24, 25]. The adapted framework showed better accuracy than the SURF-based approach in most of the datasets applied to histology and  $\mu$ CT jawbone samples. However, high computational time for dense extraction of the *SS* descriptor made it impossible to apply it to the slide-to-volume registration in its original form. Therefore the *SS* was assigned to feature points found with SURF [26]. Herein, we propose a feature detection strategy based on *SS* while diminishing dense extraction of the feature points. We achieve this aim by developing a speeded-up version of the *SS* descriptor extraction using the code provided by Chatfield et al. [27]. Our implementation allows for densely computing rotation-invariant features within a time frame of one second for the entire image with a size of  $200 \times 200$  pixels. The next contribution of this work is a modification of the matching pipeline of descriptors, in order to make it more robust. A recently proposed  $L_1$ -norm based outlier rejection finds stable correspondences between two sets of points [7]. In our work we introduce a combination of the second nearest neighbour and  $L_1$ -norm, which forms a novel feature detector self-similarity- $L_1$ -norm ( $SL_1$ ). We show that the  $SL_1$ -based framework performs equally in slide-to-volume registration and can be considered a reliable alternative in the feature-matching task. The main contribution of this study is to study its performance for multi-modal registering a histological slide to MRI and CT volume data and an slice-to-volume registration between MRI and CT datasets. We show that the initially developed framework for 2D histology to 3D  $\mu$ CT volume registration can be applied to non-invasive modalities such as MRI and CT.

## Materials and Methods

A human cerebellum block ( $6 \times 6 \times 11 \text{ mm}^3$ ) was extracted from the donated body of a 68-year-old male in accordance with the Declaration of Helsinki and according to the ethical guidelines of the Canton of Basel. The phase-contrast SR $\mu$ CT scan was performed at the beamline ID19 (ESRF, Grenoble, France), using a photon energy of 23 keV [28]. The  $\mu$ MRI dataset was acquired using a 9.4 T, 30 cm horizontal small animal MR unit (Bruker BioSpec, Bruker BioSpin MRI, Ettlingen, Germany) equipped with a transceiver cryogenic quadrature radio frequency surface coil (CryoProbeTM). For acquisition purposes a  $T_2^*$ -weighted 3D FLASH sequence with an isotropic voxel size of  $45 \mu\text{m}$  was used. Further selected parameters for the scan were: acquisition matrix  $300 \times 200 \times 300$ , echo time 12 ms, repetition time 400 ms, flip angle  $15^\circ$ , number of averages one and a total acquisition time of 400 minutes [29]. To correct the intensity inhomogeneity in the  $\mu$ MRI dataset, induced by the coil sensitivity profile, a modified fuzzy C-means algorithm was applied slice-wise [30].

Slides of the cerebellum block were prepared with a thickness of  $50 \mu\text{m}$  using a microtome with vibrating blade HM650 V (Microm International GmbH, Walldorf, Germany). The sections were mounted on gelatinized slides and stained for Nissl with cresyl violet [31]. Microphotographs of selected slices were taken using a Leica MZ16 microscope and DFC420-C digital camera.

For further analysis the 3D datasets were rigidly registered using the classical maximisation of mutual information (MI) principle [4]. Registration parameters were identified by using the Powell multi-dimensional search algorithm, such that the MI between the reference and the floating sub-images was maximised. After registering the  $\mu$ MRI, data were over-sampled along the vertical axis to  $15.3 \mu\text{m}$  as well as in horizontal axes. Hence, the final voxel size was  $15.3 \times 15.3 \times 15.3 \mu\text{m}^3$ . The  $\mu$ CT volume consisted of  $2048 \times 2048 \times 2048$  voxels with a voxel length of  $5.1 \mu\text{m}$ . For registration the dataset was binned by a factor of three, resulting in a

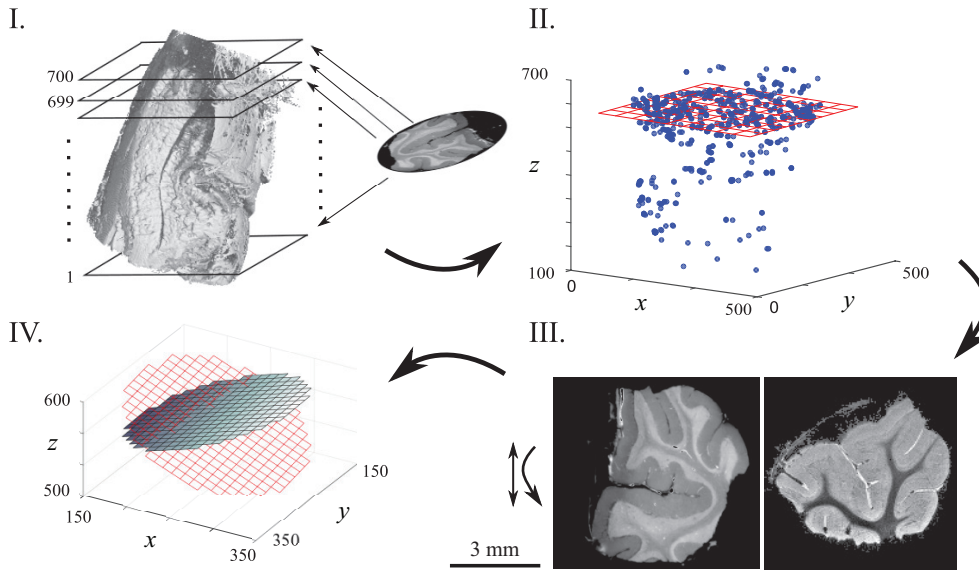


Fig 1. Slice-to-volume registration pipeline: Step I - feature matching of a 2D slice with each slice in a 3D volume; Step II - plane fitting to the 3D feature point cloud; Step III - 2D registration of the given 2D slice with an identified matching slice; Step IV - optimisation of the slice pose in 3D.

voxel length of  $15.3 \mu\text{m}$ . In addition, we filtered out bright blood intensities by thresholding ( $t = 125$ ) [29] for the matching MR data.

To register 2D slices into 3D data we used a combination of feature- and pixel-based methods (Fig. 1). The entire pipeline could be described in four steps. First, we computed matching feature points between the 2D slice and each image in the 3D dataset (Step I). Second, we fitted a plane into the 3D feature point cloud, using the modified model-fitting algorithm RANSAC [32] (Step II). Third, we rigidly registered the 2D slice and found the matching image by translating and rotating (Step III), and lastly we refined the initial position in 3D by maximising the dense similarity measure (Step IV). All the calculations were done in MATLAB on Ubuntu 15.10 with 64 GB of RAM and 12 CPUs.

### Step I. Feature matching

The 2D slices were extracted from both the MRI and the  $\mu\text{CT}$  volumes. In total, we selected 100 virtual slices from the  $\mu\text{CT}$  dataset and extracted corresponding slices from the MRI data. Three parameters were required to represent a plane in spherical coordinate system, *i.e.* distance from the origin along vertical axis, polar and azimuthal angles. We defined ten vertical positions with an interval of around 34 slices. We took ten polar angles in an interval from zero to nine degree for all slice positions except the first two and the last two slices. In that case the polar angle was from zero to three degree, because large tilting angles go beyond the limits of the 3D dataset. The 100 azimuthal angles were randomly generated withing an interval of zeros to 360 degree using uniform distribution. Therefore, for each out of ten slice positions we obtained ten tilting angles of a plane. The ground truth registration positions in the MRI dataset were estimated using known 3D transformations between the datasets.

In order to register a 2D slice extracted from, for example, an MRI dataset to a 3D  $\mu\text{CT}$  dataset, we first calculated corresponding feature points between the images (Fig. 1 (Step I)). We matched the 2D MRI image with each slice in the 3D  $\mu\text{CT}$  dataset and extracted corresponding

feature point coordinates. Based on the volume feature coordinates, the 3D point cloud was built (Fig. 1 (Step II)). Hence, the 3D dataset was now represented with a sparse point cloud which considerably reduced the complexity of registration. In the original implementation of the pipeline we used the scale- and rotation-invariant feature detector SURF [22, 26]. Here, however, due to low contrast inside the cerebellum tissue, the SURF feature points were extracted mainly from the borders of the region of interest (ROI). In order to increase the number of feature points, dense matching algorithms could be beneficial, as these approaches compute descriptor vectors on a regular grid of points and thus include landmarks of internal parts of the tissue. In a previous study by N. Khalili the *SS* descriptor showed reliable performance in slice-to-volume registration. Furthermore, in the application to multi-modal non-rigid CT-MRI registration, the *SS*-based feature detector demonstrated great potential [10]. Inspired by these works, we introduced another feature detector, namely self-similarity- $L_1$ -norm ( $SL_1$ ), and combining dense feature extraction with  $L_1$ -norm filtering allowed us to include ROI information when finding correspondences.

To calculate the *SS* descriptor for one pixel  $p = (x, y)$  of an image, two image parts centred on this pixel were required – an image patch and an image region (Fig. 2). The *SS* descriptor is a measure of a sum of squared distances (*SSDs*) between the image patch and the image region that surrounds it. *SSD* similarity within the image region builds a distance surface  $SSD_p$  at one pixel.

To account for illumination variations  $var_{noise}$  and maximal variance of intensity difference within the pixel neighbourhood  $var_{auto}$  the distance surface is divided by the maximum of these values. More precisely, the final surface is calculated as follows:

$$S_p = \exp\left(-\frac{SSD_p}{\max(var_{noise}, var_{auto})}\right). \quad (1)$$

Next, the descriptor matrix is converted to a binned log-polar representation (Fig. 2). We obtained *SS* descriptors using the public implementation made available by Chatfield et al. [27]. Obtaining these descriptors can result in significant computational cost, and this is especially time-consuming for dense feature extraction. We optimised the original code base, in order to better exploit memory locality, and tuned it to perform best for batch processing and our chosen parameter values.

Another important modification to the code provided by Chatfield et al. is the rotation invariance of the descriptor. Inspired by the SIFT orientation histograms [33], we implemented a similar idea for *SS* [24, 25] based on rotating the *SS* descriptor so that the dominant orientation for each descriptor is located at the same position. In contrast to SIFT, where the descriptor is obtained from neighbourhood gradients, here the  $S_p$  distance surface of the descriptor was used.

To register 2D point sets robustly in the presence of outliers and false correspondences, we follow a recent work by Ask et al. [7] on the exact minimisation of the truncated registration error. Given sets of corresponding feature points, this method computes optimal rotation and translation values that minimise the truncated  $L_1$  norm of the registration error. They show that the translation vector can only take on one of a finite set of values, which can be enumerated easily. Given a translation vector, the problem of finding the rotation is reduced to testing a finite set of candidate rotations that correspond to extrema of the  $L_1$  norm. Brute force iteration of these two sets is performed in  $O(n^3 \log n)$  asymptotic time, where  $n$  is a size of an input. Therefore, after extracting *SS* descriptors and matching them with second-nearest neighbour criteria (threshold = 0.8), we filter outliers from the dense correspondence with  $L_1$ -norm minimisation. As soon as the rotation and translation between the two sets of corresponding points are found, we map one set to another. By setting the threshold distance (e.g. to 10 pixels) between the mapped points, we reject points that do not satisfy this criterion. The proposed self-similarity- $L_1$ -norm ( $SL_1$ ) matching algorithm enables us to find corresponding features within the whole ROI of the image. The image patch and the image region sizes for the *SS* descriptor were set to the default

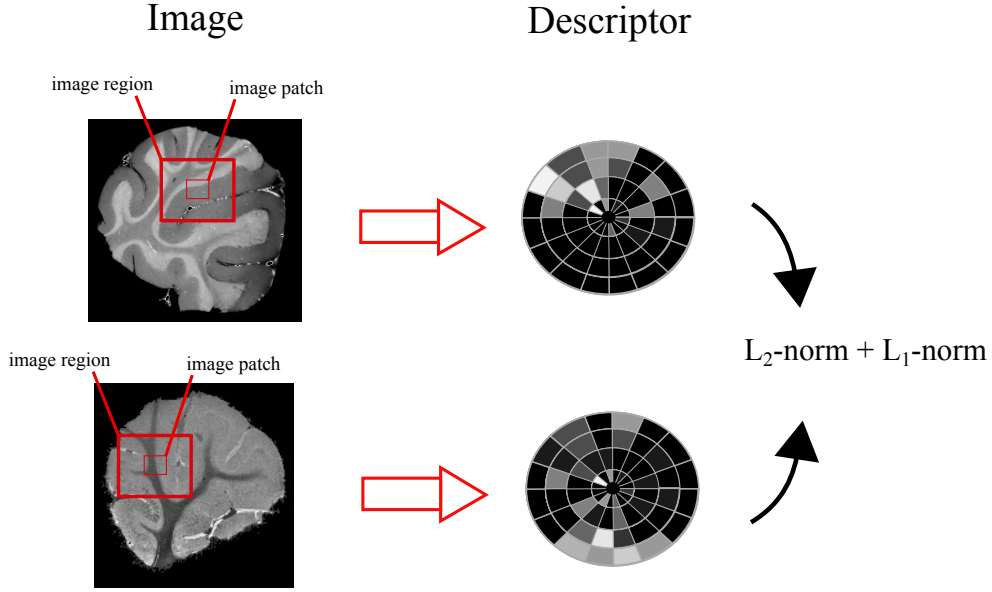


Fig 2. Calculation of the  $SL_1$  feature detector. For each pixel in an image the descriptor is calculated based on the sum of squared distances between a patch and a region (red boxes), following which the descriptor is converted to a binned log-polar coordinate system. Finally, the obtained descriptors of the two images are matched using a combination of  $L_1$  and  $L_2$  norms.

(5 pixel and 40 pixels respectively). The step size for descriptor extraction was 20 pixels in  $x$ - and  $y$ -directions of the image.

### Step II. Plane localisation

The corresponding points found for each  $\mu$ CT image (Step I) were subsequently stored in the 3D space of the  $\mu$ CT dataset. An example of a 3D point cloud is shown in Fig. 1 (Step II). One can reasonably assume that the density of the point cloud increases in the event of a correctly matching slice. Therefore, the slice-to-volume registration problem can be viewed as a density problem in 3D space. The position of a 2D section within the related volume might be approximated by a plane  $Ax + By + Cz + D = 0$ , the parameters of which need to be optimised.

To find the corresponding slice in 3D, first we filter the 3D point cloud to enhance areas with a denser distribution of corresponding points. We crop the outliers that are located further than  $M/2.2$  from the centre, where  $M$  is the size of the image in the 3D dataset. Then, we weight the points with a 3D Gaussian, and depending on the total number of points we remove the ones with the lowest weights. If the total number of points left after radial cropping is defined as  $P_{total}$ , then the final number of points with the highest weights for RANSAC fit  $P_{left}$  is calculated as

$$P_{left} = \begin{cases} P_{total} & \text{if } P_{total} < 1500 \\ 1500 & \text{if } 1500 < P_{total} < 5000 \\ P_{total}/3 & \text{if } 5000 < P_{total} < 10000 \\ P_{total}/4 & \text{if } 10000 < P_{total} < 40000 \\ 10000 & \text{if } 40000 < P_{total} \end{cases} \quad (2)$$

The thresholding values were found empirically. To find the best matching plane coefficients



we use a modified heuristic model fit approach, RANSAC [22, 32]. The weights-driven RANSAC fits a plane into the 3D cloud and chooses the one with the highest number of points. The main modification of the RANSAC is concerned with fixing the total number of iterations to 15 000 and limiting the plane tilt. This way we found a slice which was located in the densest part of the 3D cloud. The limit of the tilting angle between the normal to the plane and  $z$ -axis was set to  $\alpha = \pi/10$ .

### Step III. 2D-2D Rigid Registration

Slice localisation with the modified RANSAC gives a reasonable approximation of the correct position. Often this step is sufficient to find a reasonable registration for the given 2D image [22]. In some cases, however, an improvement of localisation through pixel-based similarity measures such as NMI or NCC is desired [34]. As a prerequisite for reliable NMI calculation, we need to register the 2D MRI image with the matching slice. Due to an insufficient ratio of correct correspondences over wrong ones for MRI and CT images, the application of RANSAC homography [32] was not reasonable. Therefore, for the 2D-2D registration we relied on the NCC as a similarity measure. As the scale for the data is given from the data preferences, in this step we needed only compensate for rotation and translation. We divided the 2D registration into two subsequent steps: rotation and translation. Let  $I : \Omega \subset R^2 \rightarrow R$  be a 2D image we want to register to the 3D volume and  $J : \Omega \subset R^2 \rightarrow R$  the matching image found above.

The images from these datasets were easily segmented from the background. The histograms of the images from both modalities had a distinctive bimodal distribution. Therefore, we used Otsu's method to automatically segment the foreground of both images [35], following which we used the binarised images to find the highest NCC for the preselected rotations. We rotated  $I^S$  from zero to  $359^\circ$  with a step of one degree and calculated the NCC between the images, before we picked the rotation angle with the highest similarity value. We defined  $I^S$  and  $J^S$  as the corresponding segmented images. The rotation matrix  $R^*$  was hence calculated as

$$R^* = \arg \max_R \text{NCC}[I^S \circ R^{-1}, J^S]. \quad (3)$$

where  $I \circ R^{-1}(\vec{x}) := I(R^{-1}\vec{x})$  and  $R$  was a rotation matrix in the space of all the rotation transformations.

Subsequently, the translation  $T^*$  of the image was determined by maximising  $\text{NCC}^1$  between the rotated images  $I_R = I \circ R^{*-1}(\vec{x})$  and extracting from the 3D data image  $J$ . Translation mapping was hence obtained as

$$T^* = \arg \max_T \text{NCC}[I_R \circ T, J], \quad (4)$$

where  $T(\vec{x}) = \vec{x} + \vec{t}$  and  $\vec{t}$  were translation vectors. The final registered image was then  $I^* = I \circ R^{*-1} \circ T^*$ .

### Step IV. Rigid 2D-3D registration

The position initialisation of the given 2D slice in a 3D volume allows for improving slice localisation by using dense similarity metrics such as NMI [36], NCC [37], MSD, etc. Our optimisation framework searched for the plane coefficients that would maximise the similarity measure. On each iteration, an image was extracted based on new plane coefficients, and the similarity was then calculated. Here we considered only rigid deformation, namely tilting and shifting of the plane. The applied optimisation algorithm was a bounded Nedler-Mead simplex<sup>2</sup>

<sup>1</sup><http://www.mathworks.com/matlabcentral/fileexchange/18401-efficient-subpixel-image-registration-by-cross-correlation>

<sup>2</sup><http://ch.mathworks.com/matlabcentral/fileexchange/8277-fminsearchbnd-fminsearchcon>

with bounding constraints of 80 slices above and below the initial position and the tilting angle was restricted to a range of  $\pm\pi/10$ . Therefore, the optimised coefficients were obtained from equation

$$n_{optim} = \arg \max_n NCC[J(n), I^*], \quad (5)$$

where  $J(n)$  is an image interpolated from the volume.

## Results

Generally, the  $SL_1$ -SURF approach with optimisation provides the best result as shown in Fig. 3 and Fig. 4. Here, the measure of the mutual information yields a maximum for the CT data with 1.118 compared to 1.069 with  $SL_1$  and 1.116 with SURF. The registration of the MRI data basically fails for SURF and  $SL_1$  (Fig. 4). But the matching slice can be found in the MRI data using the 3D pre-registered CT data and the location of the registered CT slice.  $SL_1$  improves the registration of the MRI data compared to SURF, but it is slightly the opposite for the CT data. In this case, the slice found by the Ransac algorithm with  $SL_1$  match better than the one using SURF, but the 2D-2D registration is not sufficient to provide a good starting point for the optimisation procedure. The combination of both seems to be the best choice for both modalities, while the CT slice provides the better representations. Registering the histological slide to the CT data always yields the best results using the present descriptors.

To estimate the performance of the proposed frameworks, we compared the ground truth slice parameters and those found in the 2D-3D registration method. In particular, we calculated the absolute vertical position error (Table 1) and absolute angle differences (Table 2) between normal vectors.

Table 1. Vertical position error for 3D  $\mu$ MRI and 3D  $\mu$ CT datasets in six pipeline settings [mm].

Data	Methods	SURF		$SL_1$		SURF- $SL_1$	
		NCC	NMI	NCC	NMI	NCC	NMI
CT		1.5 $\pm$ 1.1	1.6 $\pm$ 1.2	1.1 $\pm$ 0.9	1.1 $\pm$ 0.9	1.3 $\pm$ 1.1	1.5 $\pm$ 1.2
MRI		1.8 $\pm$ 1.4	1.8 $\pm$ 1.4	1.8 $\pm$ 1.6	1.8 $\pm$ 1.5	1.9 $\pm$ 1.5	1.9 $\pm$ 1.5

Table 2. Angle between normal vector values for 3D  $\mu$ MRI and 3D  $\mu$ CT datasets in six pipeline settings [degree].

Data	Methods	SURF		$SL_1$		SURF- $SL_1$	
		NCC	NMI	NCC	NMI	NCC	NMI
CT		10 $\pm$ 4.7	10 $\pm$ 4.8	7 $\pm$ 5	7 $\pm$ 5	10 $\pm$ 4.7	10 $\pm$ 4.8
MRI		5.4 $\pm$ 3.6	5 $\pm$ 3	5 $\pm$ 3	4.7 $\pm$ 3	6 $\pm$ 4	5.8 $\pm$ 4

Three different initialisation strategies in Step I and two similarity metrics in the optimised search (Step IV) were explored. The total median error for the MRI dataset was 1.9 mm and for the CT dataset was 1.3 mm. To determine whether the proposed techniques were significantly different we performed the Wilcoxon test on vertical position error values. Three groups were formed: the first group was the initialisation approaches in Step I, the second group was similarity metrics in Step IV and the third was data type (MRI or CT). As a result we found that the initialisation with  $SL_1$  was significantly better than  $SL_1$ -SURF ( $p < 0.05$ ) as well as SURF ( $p < 0.005$ ), whereas there were no difference between SURF and  $SL_1$ -SURF detectors ( $p = 0.3$ ). With a high confidence ( $p = 5 * 10^{-8}$ ) the registration of MRI slices to 3D CT dataset was better than registering CT slices to 3D MRI volume. However, no difference was found for similarity metrics in Step IV ( $p > 0.5$ ).

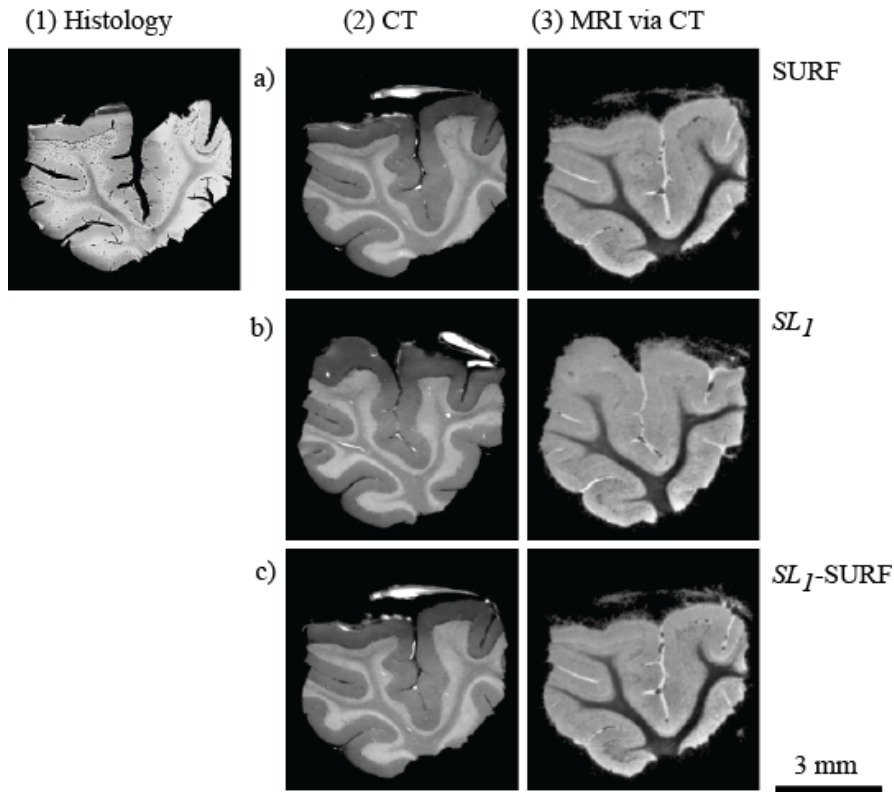


Fig 3. Registration of histological slide (1) to CT data (2) using a) SURF , b)  $SL_1$  and c)  $SL_1$ -SURF. The matching slice in the MRI data (3) is extracted in a data set pre-registered to the CT data using the plane location determined in the CT data set. In this manner a proper registration can be achieved, while the direct registration of the histological slide to the MRI data is not satisfactory (see also Fig. 4).

In Table 1 a) we can see that for the MRI volume no significant difference was found between the pipelines. Slightly better localisation of the 2D CT slices in the 3D MRI volume was achieved with the  $SL_1$ -based initialisation (Step I) as opposed to other initialisation strategies. The best performance in the 3D CT dataset was provided by the  $SL_1$  features detector and NMI similarity measure. The median error was 1 mm, achieving the smallest error among all the proposed registration techniques. Determining the plane angulation (Table 2) was significantly better with  $SL_1$  than with other detectors ( $p < 6 * 10^{-8}$ ). In contrast to distance error finding angle was significantly better in the MRI than in the CT dataset ( $p = 3 * 10^{-38}$ ). Similarly, there were no difference between NCC and NMI. The total median angle between the planes was around  $5^\circ$  for the MRI and  $9^\circ$  for the CT datasets.

In order to estimate the number of correctly registered slices we needed to account for the intrinsic properties of the 3D data. The difference in resolution in the datasets can allow for a correct registration position within a certain range. To estimate this range, we took a slice out of a volume at the centre of the vertical axis and compared it with the rest of the slices in the 3D volume. The NCC metric gives a perception of the similarity values range by setting identical slice similarity values to 1 (NCC = 1) and absolutely dissimilar ones to 0 (NCC = 0). To estimate the number of correctly registered slices, we found the slice's vertical positions at the NCC where

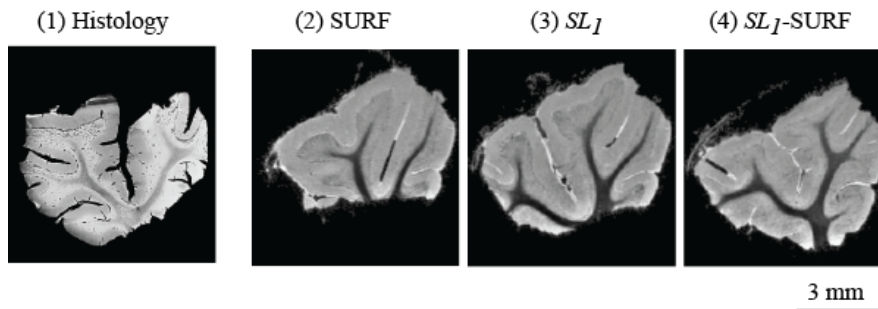


Fig 4. Registration of histological slide (1) to MRI data using SURF (2),  $SL_1$  (3) and  $SL_1$ -SURF (4). The descriptor  $SL_1$  improves the registration result compared to SURF, but the best result is provided by the consideration of both  $SL_1$  and SURF descriptors.

it drops by approximately half. We found that for our datasets the vertical position error was less than 100 slices (1.5 mm), which was acceptable. Based on the estimation of the vertical position interval, Table 3 shows the percentage of correctly registered slices for each framework.

Table 3. **Relative number of correct registrations.**

Methods	MRI with NCC	MRI with NMI	CT with NCC	CT with NMI
SURF	48%	46%	56%	56%
$SL_1$	51%	47%	79%	79%
$SL_1$ -SURF	50%	47%	67%	62%

On average the method was able to allocate more than half of the randomly selected slices. The best performance for the MRI dataset showed the  $SL_1$  feature point matching with NCC in the optimisation search. Here, 51% of the 2D CT slices were correctly localised. In the CT dataset, the best performing parameter was the  $SL_1$  based feature detector (Step I). The total number of correctly registered slices in the CT datasets was 1.4 times higher than in the MRI, which is a consequence of higher pixel resolution.

In addition to the semi-automatic algorithm evaluation we also performed manual assessment of the registration algorithms (Table 4). Here, the registration pipelines used NMI in optimization step (Step IV) and three initialization strategies in Step I: SURF,  $SL_1$  and SURF- $SL_1$ . However, in Step I we utilize the descriptors that are not invariant to rotation and, hence, relative number of correct registration using semi-automatic evaluation differs from Table 3. Three experts evaluated 100 images per dataset found using three feature detectors. A successful registration was counted as 1 and a failed registration as 0. The experts were mostly consistent in their estimates for the CT dataset. On average difference in estimation of correct registration did not exceed 2.6%. Whereas for the MRI dataset average differences between experts were 5.3%, 4.6% and 14.6% for the SURF,  $SL_1$  and SURF- $SL_1$  pipelines correspondingly. Moreover, semi-automatic performance estimation was from 15% to 25% higher than the one from the experts suggesting that the lower value would provide a better representation of the errors.

To calculate the SURF descriptor it takes approximately one second per image. The computation time of  $SL_1$  features achieves computationally fast SURF with the patch size  $5 \times 5$  pixels and  $40 \times 40$  pixels, as proposed in the original paper [38]. In order to reduce the number of feature points found with  $SL_1$  we take every 20 pixel. The entire pipeline for 2D-3D registration was performed in parallel, using the GNU Parallel software package [39]. The computation time for 2D-3D registration per one slice was around 15 minutes.

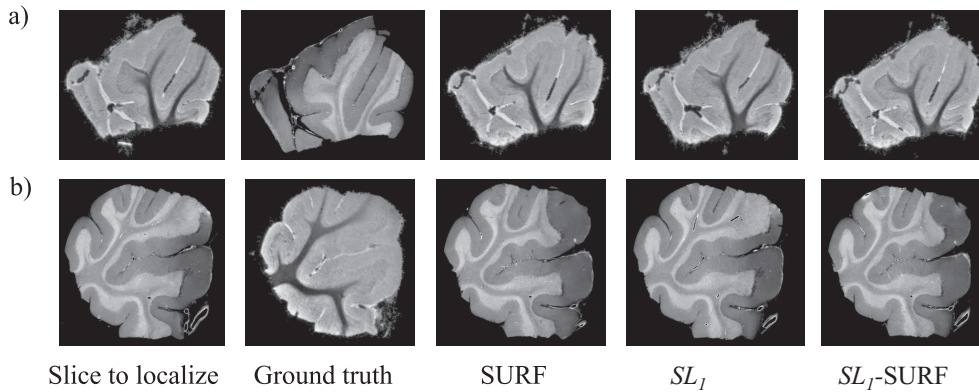


Fig 5. Examples of the registration of MRI (a) and CT (b) datasets for three pipelines: SURF,  $SL_1$  and SURF- $SL_1$  based on NCC similarity in Step IV. The first column depicts randomly extracted  $\mu$ CT (a) and  $\mu$ MRI (b) slices. The following column shows the corresponding slices in another dataset.

Table 4. **Manual evaluation of registration.**

Methods	SURF		$SL_1$		SURF- $SL_1$	
	CT	MRI	CT	MRI	CT	MRI
Expert 1	66%	67%	73%	79%	73%	76%
Expert 2	66%	63%	76%	87%	72%	73%
Expert 3	65%	59%	77%	65%	72%	80%
Semi-automatic	91%	83%	91%	92%	93%	94%

## Discussion

The registration to MRI data set is challenging to due several reasons. First, the data set features a low resolution which leads to a loss of small scale structures recognizable by the SURF descriptor. Second, the contrast between the outer brain layers is smaller. Third, blood vessels that usually lead to reliable matching points are invisible. On the other hand, the histological slide shows significant fractures as a result of the preparation and intensity gradients. Despite these artifacts the registration to the CT data set performs well due to the higher number of matching points and provides a good basis for the final determination of the matching slice in the MRI data set. Here, the 3D-3D registration of CT and MRI offers a valuable mapping that can be achieved a-priori in a reliable manner.

Locating a 2D histological slice in a 3D dataset is very challenging and mainly done manually. Manual methods, however, are time-consuming and not reproducible, which motivated us to develop an automatic solution for slice localisation in 3D space [22]. Although the slice position was calculated in a fully automatic manner, the validation of the algorithm was performed through comparison with manual coordinates, as often done in the field. This approach, however, has an apparent drawback – manual results may vary from expert to expert, so the algorithm cannot be evaluated straightforward. For example, an attempt to validate registration results with an artificially generated ground truth was made in Schnabel et al. [40]. To overcome this problem and create a fair platform for comparing different algorithms, a test dataset can be used which is pre-registered using established automatic methods. The 2D slices are then extracted randomly and the performance of 2D-3D registration algorithms is evaluated based on the known location of the slice. Similarly, herein, we validate the developed slice-to-volume registration

algorithm on already registered MRI and CT datasets calculated the errors of the algorithm, excluding any manual interactions. Moreover, we show that our pipeline can be applied to a general slice-to-volume registration problem, not only to the histology-CT data for which it was originally developed [41]. Indeed, the total median vertical position error is 1.5 mm. The smallest median error (1 mm) is observed for  $SL_1$  slice position initialisation, at the same time achieving the highest number of correctly registered slices.

Another valuable contribution of this work is a novel feature detection strategy, which we call  $SL_1$ . The feature points extracted with SURF are not able to find a sufficient gradient inside the ROI of the image. Consequently, matching with SURF is based largely on contours on the outside edge of the specimen. In contrast, the  $SL_1$  can allocate features even inside the slice ROI. Moreover, the computationally speeded-up version of  $SL_1$  makes it possible to take into account larger patch sizes. However, the computation time of the  $SL_1$  for large images is still quite high compared to the SURF. Nevertheless, for future applications, we plan to exploit the full potential of cross-correlation descriptors and investigate other matching strategies, both in 2D and 3D, to improve performance.

One of the promising improvements to the slice-to-volume registration could be associated with the shape of the specimen. Indeed, samples often have different amounts of tissue in the top and the bottom parts. Therefore, incorporating contour or shape information, so that the 3D search also depends on the size of the ROI, would be beneficial. For example, penalising a change to an ROI square, or using more sophisticated approaches to shape analysis like Procrustes analysis [42], would reduce the search space of plane parameters.

To conclude, our frameworks for 2D slide to 3D volume registration performed well for histology and  $\mu$ CT and enables the registration to MRI data which was impossible before. In addition, the automatic validation of the algorithms checked their robustness for a challenging MRI-CT correspondence problem. Furthermore, to leverage research in the field of multi-modal registration we will make publicly available the code for slice-to-volume registration as well as for the  $SL_1$  feature detector.

## **Acknowledgements**

The work was funded by Swiss National Science Foundation (SNSF) project 150164.

# Chapter 4

## Discussion

The main goal of my thesis was to develop an automatic approach to register histology images to  $\mu$ CT volumetric data. This goal was successfully accomplished by introducing a fully automatic slice-to-volume registration method [Chicherova et al., 2014, 2017b]. An important step towards this goal was the development of an extended version of a multi-modal feature detector -  $SL_1$ . This detector showed competitive results, and in our opinion, deserves further investigation.

To register a light microscopy image (e.g., a histological slide) and an X-ray tomography image, one needs first to find a robust measure of similarity. To this end, we considered the most popular multi-modal similarity measures such as normalized mutual information (NMI) and normalized cross-correlation (NCC). However, we found that these measures were not suitable for our problem because they are not invariant to rotation. Invariance to rotation is, however, a crucial property because histological slides are arbitrarily rotated. Therefore, we decided to use landmark based algorithms due to their rotation invariance and fast computation time. In particular, we chose the SIFT detector and its variations (SURF, ASIFT, etc.) because they are invariant not only to rotation but also to a large extent to contrast. Inhomogeneities of image contrast are very common and originate for example from uneven dying of histological slides. Next, we showed that from the SIFT family, the SURF was the most robust solution [Chicherova et al., 2016]. For this reason, in all our studies we used SURF as the benchmark. However, simply summing up matching SURF features per slice and then choosing the one

with the highest number of matching points was not sufficient to register a 2D slide to a 3D volume. Along with correct matching points (inliers), SURF feature matching resulted in many outliers which biased the results. The key idea to overcome this problem was complementing the pipeline with a robust RANSAC model fitting algorithm [Chicherova et al., 2014]. This enabled us to automatically localize a plane in 3D space under arbitrary tilting angles, which has never been tackled before in previous studies. Moreover, the sparse representation of the 3D volume with distinctive features markedly reduced the computation time. In a follow-up study, we tested the robustness of the developed techniques on datasets of different X-ray based modalities [Chicherova et al., 2015, 2016] and MRI [Chicherova et al., 2017a]. We showed that our method can be applied to a range of different modalities, which broadens the scope of potential applications. Importantly, the method's invariance to rotation and scale allows avoiding manual pre-processing steps and, in contrast to other approaches, no serial or multiple histology sections are needed. These properties make the method not only easily applicable but also reduce the experimental work in labor-intensive histological sectioning.

Being able to localize a slice in a 3D data volume is necessary but not sufficient to achieve a complete registration. Our initial approach [Chicherova et al., 2014] could find the place where a histological cut was most probably extracted. However, a fully-registered 2D histological image also needs to be aligned with the 2D CT slice so that one can see corresponding tissues at the same location. Therefore, we continued our research and developed a pipeline that could both improve the localization accuracy and additionally register the slice in 3D space [Chicherova et al., 2017b]. In this study, we also introduced nonlinear deformations of histological slides which often occur in soft tissue sectioning [Hieber et al., 2016, Khimchenko et al., 2016] further improving registration quality.

We also investigated a different way to improve the 2D-3D matching. In particular, we worked on optimizing the first part of the algorithm, *i.e.* the feature detection. In all previous studies, we used SURF as a feature detector to find matching points. However, using SURF might be suboptimal given the multi-modal nature of the images, because it is based on gradients which might not be similar between modalities. Thus, we decided to develop a feature detector that could better fit our needs. A Master thesis was completed on this subject in our group



---

[Khalili, 2015] based on which we developed a multi-modal alternative to SURF named  $SL_1$  [Chicherova et al., 2017a]. The  $SL_1$  is in fact a combination of the  $SS$  descriptor [Shechtman and Irani, 2007] with the  $L_1$ -norm as a cost function for robust outlier rejection. An important advantage of  $SL_1$  is its dense feature extraction. In particular, it finds significantly more feature points and correspondences in low-contrast regions, which is very advantageous when using soft, highly homogenous tissue samples such as human brain. Another important conclusion from Chicherova et al. [2017a] is that our pipeline was automatically validated excluding manual bias from the assessment.

We will make the developed slice-to-volume registration algorithm publicly available on a GitHub repository at <https://github.com>. It has already been extensively used in our group and became a routine analysis procedure in our histology projects [Thalmann et al., 2015, Hieber et al., 2014, Buscema et al., 2014, Hieber et al., 2016, Khimchenko et al., 2016]. We will also make our feature detector and descriptor  $SL_1$  open source. Although the implementation of the original  $SS$  descriptor already exists, our implementation is significantly faster which allows this descriptor to be used for high-resolution images. Apart from the  $SL_1$  descriptor which is written in C++, the pipeline is implemented in Matlab.

Future research needs to focus on further increasing the robustness of the algorithm. Often biological samples have irregular shapes that interfere with feature detection and consequently lead to registration deviations. For example in the case of dental cylindrical-shaped samples the amount of tissue may decrease around the top or bottom parts of the sample. This sometimes misleads optimization. This is likely due to the way mutual information is calculated. Specifically, when two images are almost entirely black, mutual information is very large. This is why, when calculating MI between a histology slice and an image with large background parts, the MI estimation is biased and registration is likely to converge to these low region of interest slices. Even though this occurs only for a small number of slices and can be partly eliminated by normalizing MI, future work is needed to handle these cases better. For example, one can try to include contour information in the pipeline. Contours that are very different from the histological slide contours should be penalized. The cost function could then be augmented by using NMI and a term for the distance between contours.

Another promising direction of research is to implement our pipeline in various MRI applications. Registration of histological slides to MRI data has been well studied [Ourselin et al., 2001, Ou et al., 2009]. The MRI modality is the standard choice for soft tissue investigation and can be found in many clinical applications. The existing approaches, however, do not provide fully automated solutions. We showed that our method can be applied to CT-MRI correspondence and we believe that it has the potential to improve histology to MRI registration as well.

Independently of the main pipeline, an extension of the  $SS$ -based detector, namely  $SL_1$ , deserves further investigation. The application to other types of images and an extensive comparison with existing detectors could unravel its limitations and advantages.

# Bibliography

- L. Alic, J. C. Haeck, K. Bol, S. Klein, S. T. van Tiel, P. A. Wielepolski, M. de Jong, W. J. Niessen, M. Bernsen, and J. F. Veenland. Facilitating tumor functional assessment by spatially relating 3D tumor histology and *in vivo* MRI: Image registration approach. *PLoS One*, 6(8):e22835, 2011.
- A. Andronache, M. von Siebenthal, G. Székely, and P. C. Cattin. Non-rigid registration of multi-modal images using both mutual information and cross-correlation. *Medical Image Analysis*, 12(1):3–15, 2008.
- I. Arganda-Carreras, R. Fernández-González, A. Muñoz-Barrutia, and C. Ortiz-De-Solorzano. 3D reconstruction of histological sections: Application to mammary gland tissue. *Microscopy Research and Technique*, 73(11):1019–1029, 2010.
- E. Ask, O. Enqvist, L. Svärm, F. Kahl, and G. Lippolis. Tractable and reliable registration of 2D point sets. *Lecture Notes in Computer Science*, 8689:393–406, 2014.
- M. S. Breen, R. S. Lazebnik, and D. L. Wilson. Three-dimensional registration of magnetic resonance image data to histological sections with model-based evaluation. *Annals of Biomedical Engineering*, 33(8):1100–1112, 2005.
- E. Bullitt, A. Liu, S. R. Aylward, C. Coffey, J. Stone, S. K. Mukherji, K. E. Muller, and S. M. Pizer. Registration of 3D cerebral vessels with 2D digital angiograms: Clinical evaluation. *Academic Radiology*, 6(9):539–546, 1999.
- M. Buscema, M. N. Holme, H. Deyhle, G. Schulz, R. Schmitz, P. Thalmann, S. E. Hieber,

- N. Chicherova, P. C. Cattin, F. Beckmann, et al. Grating interferometry-based phase microtomography of atherosclerotic human arteries. *Proc. SPIE*, pages 921203–921203, 2014.
- N. Chicherova, K. Fundana, B. Müller, and P. C. Cattin. Histology to  $\mu$ CT data matching using landmarks and a density biased ransac. *Lecture Notes in Computer Science*, 8673: 243–250, 2014.
- N. Chicherova, P. Cattin, G. Schulz, K. Fundana, B. Müller, and S. E. Hieber. Automatic matching of grating-based phase tomography dataset with histology. *European Cells and Materials*, 30:34, 2015.
- N. Chicherova, S. E. Hieber, G. Schulz, A. Khimchenko, C. Bikis, P. C. Cattin, and B. Müller. Automatic histology registration in application to X-ray modalities. *Proc. SPIE*, pages 996708–996708, 2016.
- N. Chicherova, S. E. Hieber, B. Bitterli, G. Schulz, P. C. Cattin, and B. Müller. Automatic 2D-3D registration of histology, MRI and CT data. *Biomedical Optics Express*, unpublished, 2017a.
- N. Chicherova, S. E. Hieber, A. Khimchenko, C. Bikis, B. Müller, and P. C. Cattin. Automatic deformable registration of histological slides to  $\mu$ CT volume data. *Journal of Microscopy*, unpublished, 2017b.
- J. Dauguet, T. Delzescaux, F. Condé, J.-F. Mangin, N. Ayache, P. Hantraye, and V. Frouin. Three-dimensional reconstruction of stained histological slices and 3D non-linear registration with *in-vivo* MRI for whole baboon brain. *Journal of Neuroscience Methods*, 164(1):191–204, 2007.
- A. du Bois d’Aische, M. De Craene, X. Geets, V. Gregoire, B. Macq, and S. K. Warfield. Efficient multi-modal dense field non-rigid registration: alignment of histological and section images. *Medical Image Analysis*, 9(6):538–546, 2005.
- B. Fei, J. L. Duerk, D. T. Boll, J. S. Lewin, and D. L. Wilson. Slice-to-volume registration and its potential application to interventional MRI-guided radio-frequency thermal ablation of prostate cancer. *Medical Imaging, IEEE Transactions on*, 22(4):515–525, 2003.

- M. A. Fischler and R. C. Bolles. Random sample consensus: a paradigm for model fitting with applications to image analysis and automated cartography. *Communications of the ACM*, 24:381–395, 1981.
- M. Goubran, C. Crukley, S. de Ribaupierre, T. M. Peters, and A. R. Khan. Image registration of *ex-vivo* MRI to sparsely sectioned histology of hippocampal and neocortical temporal lobe specimens. *NeuroImage*, 83:770–781, 2013.
- M. Goubran, S. de Ribaupierre, R. R. Hammond, C. Currie, J. G. Burneo, A. G. Parrent, T. M. Peters, and A. R. Khan. Registration of *in-vivo* to *ex-vivo* MRI of surgically resected specimens: A pipeline for histology to *in-vivo* registration. *Journal of Neuroscience Methods*, 241:53–65, 2015.
- M. P. Heinrich, M. Jenkinson, M. Bhushan, T. Matin, F. V. Gleeson, M. Brady, and J. A. Schnabel. MIND: Modality independent neighbourhood descriptor for multi-modal deformable registration. *Medical Image Analysis*, 16(7):1423–1435, 2012.
- S. E. Hieber, A. Stalder, B. Ilgenstein, N. Chicherova, H. Deyhle, F. Beckmann, S. Stbinger, B. von Rechenberg, and B. Müller. Assessment of bone grafting materials in oral surgery. *European Cells and Materials*, 28:18, 2014.
- S. E. Hieber, C. Bikis, A. Khimchenko, G. Schweighauser, N. Chicherova, G. Schulz, and B. Müller. Tomographic brain imaging with nucleolar detail and automatic cell counting. *Scientific Reports*, 6:32156, 2016.
- R. M. Hoerth, D. Baum, D. Knötel, S. Prohaska, B. M. Willie, G. N. Duda, H.-C. Hege, P. Fratzl, and W. Wagermaier. Registering 2D and 3D imaging data of bone during healing. *Connective Tissue Research*, 56(2):133–143, 2015.
- J. Humm, D. Ballon, Y. Hu, S. Ruan, C. Chui, P. Tulipano, A. Erdi, J. Koutcher, K. Zakian, M. Urano, et al. A stereotactic method for the three-dimensional registration of multi-modality biologic images in animals: NMR, PET, histology, and autoradiography. *Medical Physics*, 30(9):2303–2314, 2003.

- N. Khalili. Multi-modal matching of 2-dimensional images with 3-dimensional data. *Master thesis*, 2015.
- A. Khimchenko, H. Deyhle, G. Schulz, G. Schweighauser, J. Hench, N. Chicherova, C. Bikis, S. E. Hieber, and B. Müller. Extending two-dimensional histology into the third dimension through conventional micro computed tomography. *NeuroImage*, 139:26–36, 2016.
- B. Kim, J. L. Boes, K. A. Frey, and C. R. Meyer. Mutual information for automated unwarping of rat brain autoradiographs. *NeuroImage*, 5(1):31–40, 1997.
- T.-S. Kim, M. Singh, W. Sungkara, C. Zarow, and H. Chui. Automatic registration of post-mortem brain slices to MRI reference volume. *Nuclear Science, IEEE Transactions on*, 47(4):1607–1613, 2000.
- J. Kybic and M. Unser. Fast parametric elastic image registration. *Image Processing, IEEE Transactions on*, 12(11):1427–1442, 2003.
- R. S. Lazebnik, T. L. Lancaster, M. S. Breen, J. S. Lewin, and D. L. Wilson. Volume registration using needle paths and point landmarks for evaluation of interventional MRI treatments. *Medical Imaging, IEEE Transactions on*, 22(5):653–660, 2003.
- G. Li, S. Nikolova, and R. Bartha. Registration of *in vivo* magnetic resonance  $T_1$ -weighted brain images to triphenyltetrazolium chloride stained sections in small animals. *Journal of Neuroscience Methods*, 156(1):368–375, 2006.
- F. Maes, A. Collignon, D. Vandermeulen, G. Marchal, and P. Suetens. Multimodality image registration by maximization of mutual information. *Medical Imaging, IEEE Transactions on*, 16(2):187–198, 1997.
- P. Markelj, D. Tomaževič, B. Likar, and F. Pernuš. A review of 3D/2D registration methods for image-guided interventions. *Medical Image Analysis*, 16(3):642–661, 2012.
- C. R. Meyer, B. A. Moffat, K. Kuszpit, P. L. Bland, T. Chenevert, A. Rehemtulla, and B. Ross. A methodology for registration of a histological slide and *in vivo* MRI volume based on optimizing mutual information. *Molecular Imaging*, 5(1):16, 2006.

- K. Mosaliganti, T. Pan, R. Ridgway, R. Sharp, L. Cooper, A. Gulacy, A. Sharma, O. Irfanoglu, R. Machiraju, T. Kurc, A. de Bruin, P. Wenzel, G. Leone, J. Saltz, and K. Huang. An imaging workflow for characterizing phenotypical change in large histological mouse model datasets. *Journal of biomedical informatics*, 41(6):863–873, 2008.
- G. Nir, R. S. Sahebjavaher, P. Kozlowski, S. D. Chang, E. C. Jones, S. L. Goldenberg, and S. E. Salcudean. Registration of whole-mount histology and volumetric imaging of the prostate using particle filtering. *IEEE transactions on medical imaging*, 33(8):1601–1613, 2014.
- S. Osechinskiy and F. Kruggel. Slice-to-volume nonrigid registration of histological sections to MR images of the human brain. *Anatomy Research International*, Article ID 287860, 2010.
- Y. Ou, D. Shen, M. Feldman, J. Tomaszewski, and C. Davatzikos. Non-rigid registration between histological and MR images of the prostate: A joint segmentation and registration framework. *IEEE Computer Vision and Pattern Recognition Workshops*, pages 125–132, 2009.
- S. Ourselin, E. Bardinet, D. Dormont, G. Malandain, A. Roche, N. Ayache, D. Tande, K. Parain, and J. Yelnik. Fusion of histological sections and MR images: towards the construction of an atlas of the human basal ganglia. *Lecture Notes in Computer Science*, 2208:743–751, 2001.
- H. Park, M. R. Piert, A. Khan, R. Shah, H. Hussain, J. Siddiqui, T. L. Chenevert, and C. R. Meyer. Registration methodology for histological sections and *in vivo* imaging of human prostate. *Academic Radiology*, 15(8):1027–1039, 2008.
- A. Pitiot, G. Malandain, E. Bardinet, and P. M. Thompson. Piecewise affine registration of biological images. *Biomedical Image Registration*, pages 91–101, 2003.
- J. P. Plum, J. A. Maintz, and M. Viergever. Mutual-information-based registration of medical images: a survey. *Medical Imaging, IEEE Transactions on*, 22(8):986–1004, 2003.
- H. Sarve, J. Lindblad, and C. B. Johansson. Registration of 2D histological images of bone implants with 3D SR $\mu$ CT volumes. *Advances in Visual Computing*, pages 1071–1080, 2008.



- T. Schormann and K. Zilles. Three-dimensional linear and nonlinear transformations: an integration of light microscopical and MRI data. *Human Brain Mapping*, 6:339–347, 1998.
- T. Schormann, A. Dabringhaus, and K. Zilles. Statistics of deformations in histology and application to improved alignment with MRI. *Medical Imaging, IEEE Transactions on*, 14(1):25–35, 1995.
- G. Schulz, T. Weitkamp, I. Zanette, F. Pfeiffer, F. Beckmann, C. David, S. Rutishauser, E. Reznikova, and B. Müller. High-resolution tomographic imaging of a human cerebellum: comparison of absorption and grating-based phase contrast. *Journal of The Royal Society Interface*, 7:1665–1676, 2010.
- M. Seise, T. Alhonnoro, M. Kolesnik, et al. Interactive registration of 2D histology and 3D CT data for assessment of radiofrequency ablation treatment. *Journal of Pathology Informatics*, 2:9, 2011.
- E. Shechtman and M. Irani. Matching local self-similarities across images and videos. *Proceedings of the Conference on Computer Vision and Pattern Recognition*, pages 1–8, 2007.
- A. K. Stalder, B. Ilgenstein, N. Chicherova, H. Deyhle, F. Beckmann, B. Müller, and S. E. Hieber. Combined use of micro computed tomography and histology to evaluate the regenerative capacity of bone grafting materials. *International Journal of Materials Research*, 105(7):679–691, 2014.
- L. S. Taylor, B. C. Porter, G. Nadasdy, P. A. di SantAgnese, D. Pasternack, Z. Wu, R. B. Baggs, D. J. Rubens, and K. J. Parker. Three-dimensional registration of prostate images from histology and ultrasound. *Ultrasound in Medicine & Biology*, 30(2):161–168, 2004.
- P. Thalmann, A. Stalder, B. Ilgenstein, N. Chicherova, H. Deyhle, F. Beckmann, B. Müller, and S. E. Hieber. Combination of micro computed tomography and histology for the investigation of bone grafting. *European Cells and Materials*, 30:67, 2015.
- M. Uberti, Y. Liu, H. Dou, R. L. Mosley, H. E. Gendelman, and M. Boska. Registration of *in vivo* MR to histology of rodent brains using blockface imaging. *Proc. SPIE*, pages 726213–726213, 2009.

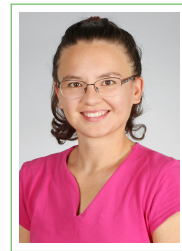
- P. Viola and W. M. Wells III. Alignment by maximization of mutual information. *International Journal of Computer Vision*, 24(2):137–154, 1997.
- M. P. Wachowiak, R. Smolíková, Y. Zheng, J. M. Zurada, and A. S. Elmaghraby. An approach to multimodal biomedical image registration utilizing particle swarm optimization. *Evolutionary Computation, IEEE Transactions on*, 8(3):289–301, 2004.
- J. Yelnik, E. Bardinet, D. Dormont, G. Malandain, S. Ourselin, D. Tandé, C. Karachi, N. Ayache, P. Cornu, and Y. Agid. A three-dimensional, histological and deformable atlas of the human basal ganglia. I. Atlas construction based on immunohistochemical and MRI data. *NeuroImage*, 34(2):618–638, 2007.
- Y. Zhan, Y. Ou, M. Feldman, J. Tomaszewski, C. Davatzikos, and D. Shen. Registering histologic and MR images of prostate for image-based cancer detection. *Academic Radiology*, 14(11):1367–1381, 2007.

# Natalia Chicherova

Strassburgerallee 87  
4055 Basel, Switzerland

+41 78 7909791

✉ natalia.chicherova@unibas.ch



## Education

- 2016–now **Postdoctoral fellow**,  
*Biozentrum, University of Basel, Switzerland.*
- 2013–2016 **Ph.D. in Medical and Biological Sciences**,  
*Department of Biomedical Engineering, University of Basel, Switzerland.*
- 2003–2009 **B.Sc. and M.Sc. in Applied Mathematics and Physics**,  
*Moscow Institute of Physics and Technology, Department of Molecular and Biological Physics, Moscow.*

## Work Experience and Projects

- 2016–now **Project 1. Microscopy data analysis**, *Biozentrum, University of Basel, Switzerland.*  
I am part of a team working on 3D visualization of bacteria and parasites
- contributing to the microscopy data visualization software development <https://github.com/Fouga/StitchIt>
    - developing algorithms to reduce image acquisition artifacts
    - cell, bacteria and organ segmentation using machine learning, convolutional neural network
    - statistical analysis, filtering and visualization of annotated data
  - facilitating and optimizing data analysis in the lab
    - programming in R and Matlab
    - analysis automatization
    - parallel computing implementation
- 2013-2016 **Project 2. Biomedical engineering**, *Department of Biomedical Engineering, University of Basel, Switzerland.*  
I developed an algorithm for 2D histological images to 3D micro Computed Tomography registration
- integrated and modified state-of-the-art feature detectors to solve slice-to-volume registration
  - had extensive experience in MatLab programming, in particular Image analysis and statistical toolboxes
  - learned the fundamentals of phase-contrast imaging as well as histological sectioning
- 2012–2013 **Research assistant**, *Swiss Institute of Bioinformatics, Lausanne.*  
Statistical analysis of colon cancer genomic data
- frequency, survival analysis, multivariable logistic regression
  - microarray analysis
  - programming in R
- 2009-2012 **Child care.**

## Computer skills

Programming **Matlab** (expert), **R** (intermediate), **Python** (intermediate)  
Software **MS Office, ImageJ, Arivis, Inkscape, Orbit, Imaris, Omero, L<sup>A</sup>T<sub>E</sub>X**

## Languages and Personal information

English	<b>Advanced (C2)</b>	Permit	<b>Eligible to work in Switzerland (Permit B)</b>
German	<b>Intermediate (B2)</b>		
French	<b>Intermediate (B1)</b>	Citizenship	<b>Russia</b>
Russian	<b>Native</b>		
Web	<b>LinkedIn, GitHub</b>		

## Extracurricular activities

- 2014–2016 **Executive member, MICCAI student board.**
- o organization of student events during MICCAI conference
  - o home web page support <http://www.miccai2014.org/edu/>

## Publications

Christos Bikis, Philipp Janz, Georg Schulz, Gabriel Schweighauser, Jürgen Hench, Peter Thalmann, Hans Deyhle, Natalia Chicherova, Alexander Rack, Anna Khimchenko, Simone Hieber, Luigi Mariani, Carola Haas, and Bert Müller. High-resolution synchrotron radiation-based phase tomography of the healthy and epileptic brain. In *Proceedings of SPIE*, pages 996706–996706, 2016.

Marzia Buscema, Margaret N Holme, Hans Deyhle, Georg Schulz, Rüdiger Schmitz, Peter Thalmann, Simone E Hieber, Natalia Chicherova, Philippe C Cattin, Felix Beckmann, Julia Herzen, Timm Weitkamp, Till Saxer, and Bert Müller. Grating interferometry-based phase microtomography of atherosclerotic human arteries. In *Proceedings of SPIE*, pages 921203–921203, 2014.

Natalia Chicherova, Philippe Cattin, Georg Schulz, Ketut Fundana, Bert Müller, and Simone E. Hieber. Automatic matching of grating-based phase tomography dataset with histology. *European Cells and Materials*, 30:34, 2015.

Natalia Chicherova, Simone E. Hieber, Benedikt Bitterli, Georg Schulz, Philippe C. Cattin, and Bert Müller. Automatic 2D-3D registration of histology, MRI and CT data. *Computers in Biology and Medicine*, unpublished.

Natalia Chicherova, Simone E. Hieber, Anna Khimchenko, Christos Bikis, Bert Müller, and Philippe C. Cattin. Automatic deformable registration of histological slides to  $\mu$ CT volume data. *Journal of Microscopy*, 271:49–61, 2018.

Natalia Chicherova, Simone E Hieber, Georg Schulz, Anna Khimchenko, Christos Bikis, Philippe C Cattin, and Bert Müller. Automatic histology registration in application to X-ray modalities. In *Proceedings of SPIE*, pages 996708–996708, 2016.

Natlia Chicherova, Ketut Fundana, Bert Müller, and Philippe C. Cattin. Histology to  $\mu$ CT data matching using landmarks and a density biased RANSAC. In *Lecture Notes in Computer Science, MICCAI*, pages 243–250. Springer, 2014.

AV. Glukhov, AV. Reznik, NV. Kovalenko(Chicherova), UV. Egorov, and LV. Rozenshtraukh. Effect of nibentan on dispersion of repolarization of ventricular myocardium in the rabbit. *Kardiologija*, 48(7):40–47, 2007.

Simone E Hieber, Christos Bikis, Anna Khimchenko, Georg Schulz, Hans Deyhle, Peter Thalmann, Natalia Chicherova, Alexander Rack, Marie-Christine Zdora, Irene Zanette, Gabriel Schweighauser, Jürgen Hench, and Bert Müller. Computational cell quantification in the human brain tissues based on hard X-ray phase-contrast tomograms. In *Proceedings of SPIE*, pages 99670K–99670K, 2016.

Simone E Hieber, Christos Bikis, Anna Khimchenko, Gabriel Schweighauser, Jürgen Hench, Natalia Chicherova, Georg Schulz, and Bert Müller. Tomographic brain imaging with nucleolar detail and automatic cell counting. *Scientific reports*, 6:32156, 2016.

Anna Khimchenko, Christos Bikis, Gabriel Schweighauser, Jürgen Hench, Alexandra-Teodora Joita-Pacureanu, Peter Thalmann, Hans Deyhle, Bekim Osmani, Natalia Chicherova, Simone E. Hieber,

Peter Cloetens, Magdalena Müller-Gerbl, Georg Schulz, and Bert Müller. Imaging cellular and subcellular structure of human brain tissue using micro computed tomography. In *Proceedings of SPIE*, volume 10391, pages 10391–10391–12, 2017.

Anna Khimchenko, Hans Deyhle, Georg Schulz, Gabriel Schweighauser, Jürgen Hench, Natalia Chicherova, Christos Bikis, Simone E. Hieber, and Bert Müller. Extending two-dimensional histology into the third dimension through conventional micro computed tomography. *Neuroimage*, 139:26–36, 2016.

Anna Khimchenko, Georg Schulz, Christos Bikis, Hans Deyhle, Natalia Chicherova, Simone E. Hieber, Gabriel Schweighauser, Jürgen Hench, and Bert Müller. Three-dimensional imaging of human brain tissues using absorption-contrast high-resolution x-ray tomography. In *Proceedings of SPIE*, volume 10162, pages 10162–10162–8, 2017.

Anja K Stalder, Bernd Ilgenstein, Natalia Chicherova, Hans Deyhle, Felix Beckmann, Bert Müller, and Simone E Hieber. Combined use of micro computed tomography and histology to evaluate the regenerative capacity of bone grafting materials. *International Journal of Materials Research*, 105(7):679–691, 2014.